Communications
Research
Centre

STABILITY ANALYSIS OF FLEXIBLE
SPACECRAFT WITH PID CONTROLLER

by

J. de Lafontaine

Government of Canada
Department of Communications

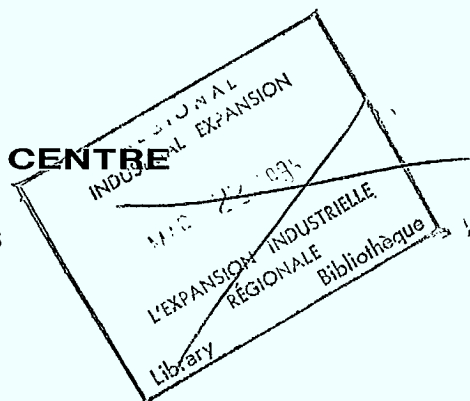Gouvernement du Canada
Ministère des Communications

Canadä

COMMUNICATIONS RESEARCH CENTRE
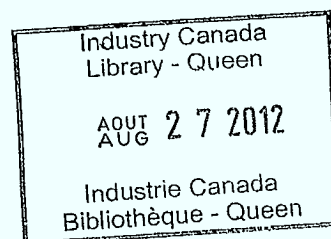
DEPARTMENT OF COMMUNICATIONS
CANADA

STABILITY ANALYSIS OF FLEXIBLE
SPACECRAFT WITH PID CONTROLLER

by

J. de Lafontaine

(Space Technology and

Applications Branch)

CRC REPORT NO. 1372

November 1984

OTTAWA

CAUTION

This information is furnished with the express understanding that:
Proprietary and patent rights will be protected.

Contents

List of Symbols

a_n, b_n, c_n :   coefficients of $F(K_p'')$ for the damped mode, Eq. (45)

a_n', b_n', c_n':   coefficients of $F'(K_p'')$ for the undamped mode, Eq. (46)

f_{DYN}, f_{SYS}:   the 'dynamics' and 'system' functions, Eqs. (6) and (19)

g :   wheel speed feedback gain

j : $= \sqrt{-1}$

k_n :   non-dimensional gain for unconstrained mode n

k_L :   equivalent gain for torque limiter

p :   product of ω_m and ω_f, Eq. (8)

p_L :   product of ω_{mL} and ω_f, Eq. (72)

s :   Laplace variable

z_n : $2\zeta_n \omega_n$

CE :   Characteristic Equation

$D(s)$:   transfer function for the system dynamics

$F(K_p'')$:   stability function for a damped mode, Eq. (45)

$F'(K_p'')$:   stability function for an undamped mode, Eq. (46)

I :   inertia about one of the spacecraft axis

K :   controller gain

K_D :   derivative gain

K_I :   integral gain

K_p :   proportional gain

K_D', K_I', K_p' :   gains multiplied by K_f/I, Eq. (8)

K_D^*, K_I^* : derivative and integral gains ratios, Eqs. (16)

K_p'' : controller (proportional) gain parameter, Eq. (14)

K_{pc}'' : critical gain K_p''

K_f : flexibility/noise filter gain, Eq. (8)

K_n : non-dimensional gain for constrained mode n

M : defined in Eq. (56)

$P(s)$: transfer function for the system controller

T : delay in seconds

T_M : wheel torque output

T_c : wheel torque demand

α : real part of the unconstrained transfer function $D(j\omega)$, Eq. (9b)

α_c : constrained equivalent of α, Eq. (24)

β : negative imaginary part of the unconstrained transfer function $D(j\omega)$, Eq. (9b)

β_c : constrained equivalent of β, Eq. (24)

γ : real part of the transfer function $KP(j\omega)$ multiplied by λ, Eq. (9a)

δ : imaginary part of the transfer function $KP(j\omega)$ multiplied by λ, Eq. (9a)

δ^* : $= \delta/\omega$

δ_x^* : δ^* evaluated at $\omega=\omega_x$

ε : tolerance

ζ_n : unconstrained damping ratio for mode n

θ : pointing angle for a given spacecraft axis

λ : defined in Eq. (10)

σ : sum of ω_m and ω_f, Eq. (8)

σ_L : sum of ω_{mL} and ω_f, Eq. (72)

τ_f : flexibility/noise filter time constant

τ_w : wheel friction time constant

ω : frequency in rad/s

ω_{ck} : k^{th} critical frequency, Eq. (51)

ω_f : flexibility/noise filter break frequency

ω_m : defined in Eq. (8)

ω_{mL} : defined in Eq. (71)

ω_n : unconstrained frequency for mode n

ω_x : frequency at which the root locus crosses the imaginary axis

ω_{xc} : crossing frequency associated with the critical frequency

ω_{xn} : crossing frequency associated with mode n

Δ : denominator of the system function, Eqs. (14) and (19)

Δ_n : denominators in the terms of α and β, Eq. (10)

Δ_T : same as Δ but for the system with delay T

Z_n : constrained damping ratio for mode n

Λ_{PD} : proportional-derivative gain function, Eqs. (10)

Λ_{PI} : proportional-integral gain function, Eqs. (10)

Ω_n : constrained frequency for mode n

List of Figures

ABSTRACT

This study presents a graphical method for the design and analysis of a flexible spacecraft controller. It can handle as many modes as desired, in constrained or unconstrained form; modal separability is not assumed and the method is exact when the spacecraft axes are uncoupled. The definition of a 'system function', independent of the controller parameters, simplifies the determination of the system stability boundaries. It also allows the investigation of the modal separability assumption, resulting in a criterion for its validity. Stabilization through structural damping and flexible modes filtering is illustrated using graphs of the system function. Closed-form approximations are derived in order to complement the exact, numerical method. Extensions to systems with loop delay and nonlinear elements are also included along with applications to the LSAT-1 Roll axis.

1. Introduction

This study presents a method for determining the stability of a PID-controlled flexible spacecraft in terms of stability diagrams in the controller parameter space. It is an extension to the work by Hughes and Abdel-Rahman[1] and was used by the present author in the investigation of the LSAT/MSAT Normal Mode performance [2]. As this reference concentrated on practical results, it was felt that it should be complemented by the mathematical background at its origin. This will allow possible usage or extension of the method to cope with other control system problems.

Extensions to Reference [2] were carried out by the author and are reported here. In particular, the definition of a 'system function', typical to a given spacecraft, makes the method general enough to accommodate dynamics models with any number of constrained or unconstrained modes.

The assumptions and the basic system model are first defined. Then, the development of the theory is carried out with numerical examples based on LSAT-1 parameters. Approximate analytical results are also introduced to help interpret the numerical approach. An extension of the method to systems with loop delay and torque limiters will complete this presentation.

2. Assumptions and System Model

The uncoupling of all three spacecraft axes is assumed throughout this work. In theory, this assumption is not valid for most spacecraft but in practice, the coupling can be so weak that this simplification is acceptable for design purposes. Each axis can thus be controlled independently as shown in Fig. 1. The saturation element allows for torque input limitation while the term e^{-Ts} considers controller processing and sensor sampling delays. The first-order filter $(1+\tau_f s)^{-1}$ accounts for noise filtering or flexible modes filtering, according to the choice of τ_f. Although the basic approach to be described is valid for various types of controllers, it is implemented here with a PID compensator. It is completely characterized by 3 parameters: the derivative K_D, proportional K_p and integral K_I gains. The method will define stability regions in the space generated by these parameters. In general, K_p is the variable gain while the ratios K_D/K_p and K_I/K_p are kept at some predetermined value.

This form of control is chosen not only because it represents a simplified version of all three axes of LSAT (see [2] for the correspondence) but also because it is considered general enough to represent most satellite of this class, including lead-lag controllers [1,3]. In the case of LSAT, higher-order flexibility filters are added to the design. This would increase the stability margins derived in the present work.

In the following sections, some additional assumptions are resorted to. Loop delay and torque limiters are avoided until the last section. Mode separability is also invoked when analytical results are sought. These simplifying steps will allow a better understanding and an easier interpretation of the more complex, original model.
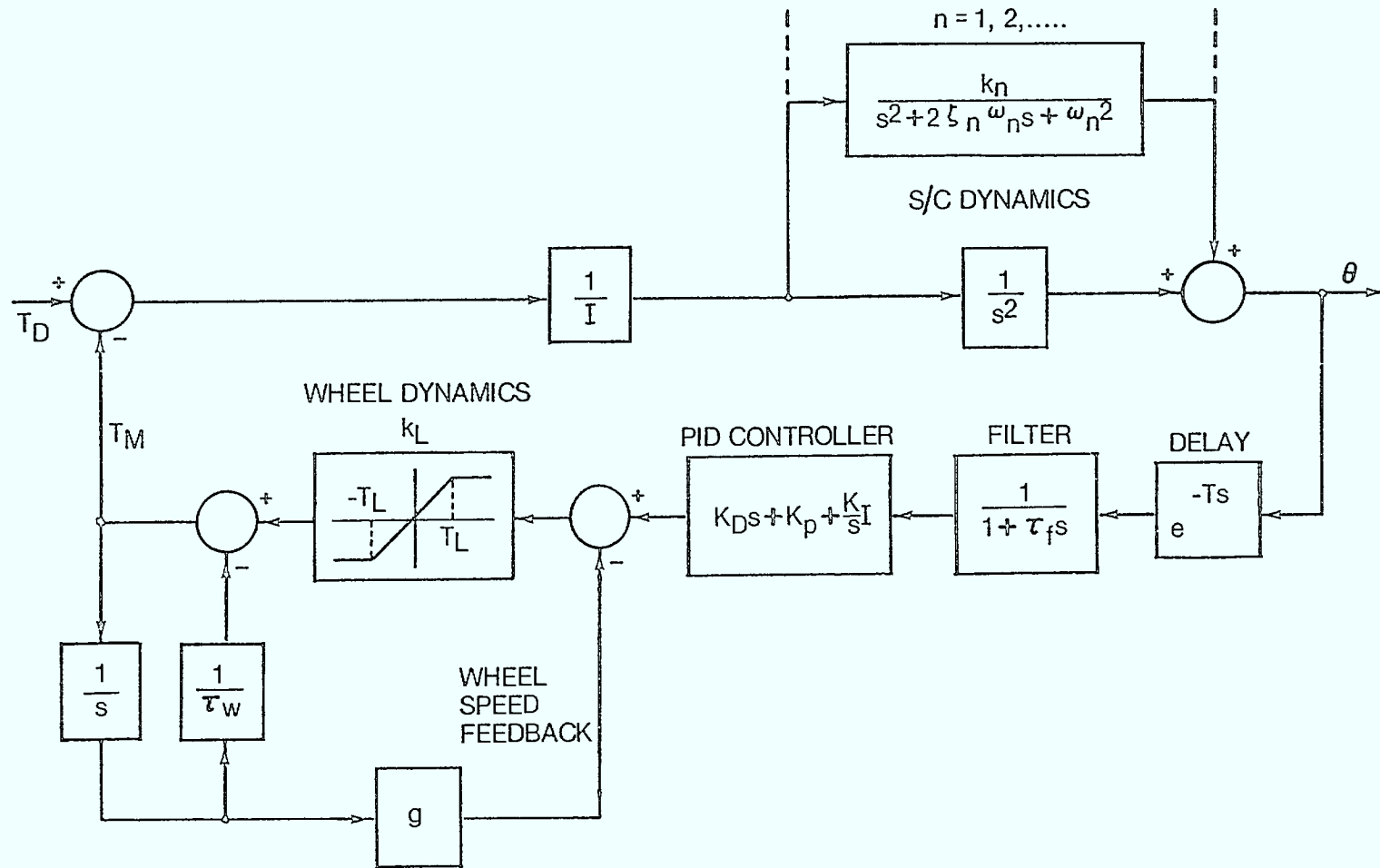
Figure 1   The Control Loop for a Single Axis

3. Development of the Stability Boundary Equations

The theoretical background for reference [2] is now presented. It is an exact method, given that axis decoupling applies.

a. Method

The open-loop transfer function of a controlled dynamical system can be written as

$$K \ P(s) \ D(s) \tag{1}$$

with $P(s)$ containing all the control parameters, $D(s)$ representing the dynamics of the plant to be controlled and K is the controller gain. The characteristic equation (CE) becomes $1 + K \ P(s) \ D(s) = 0$. The choice of control parameters that will locate roots of the CE on the imaginary axis of the s-plane will define the locus of the stability boundary in the parameter space. When this happens, the CE takes the form

$$1 + K \ P(j\omega) \ D(j\omega) = 0. \tag{2}$$

This equation can be separated into its real and imaginary parts by defining:

$$P(j\omega) \triangleq p_r + j \ p_i,$$

$$D(j\omega) \triangleq d_r - j \ d_i, \tag{3}$$

$$j = \sqrt{-1} \ .$$

Equation (2) splits into:

$$1 + K \ (p_r d_r + p_i d_i) = 0,$$

$$p_i d_r = p_r d_i \ . \tag{4}$$

So far, this derivation follows that in [1]. However, it is not easy to solve for Eqs. (4) in the present form. We wish to separate the fixed physical and modal quantities from the adjustable controller quantities. This will be done in order to simplify the solution of (4) while providing a better understanding of the problem. There exist many ways of performing this separation. For instance, one could rewrite Eqs. (4) as:

$$f_{DYN} = -1/(K p_r) \tag{5a}$$

$$d_i/d_r = p_i/p_r \tag{5b}$$

with the 'dynamics function' defined as

$$f_{DYN} \triangleq (d_i^2 + d_r^2)/d_r \quad . \tag{6}$$

This function depends on the spacecraft modal parameters alone. Hence $f_{DYN}(\omega)$ is specific to a given spacecraft and can be plotted versus frequency. Everytime this plot crosses the $-1/(Kp_r)$ curve, the corresponding frequency ω_x can be substituted into $d_i(\omega)/d_r(\omega)$ of Eq. (5b) to yield a relationship between the controller parameters p_i/p_r. These, in turn, define the stability boundary. Note that ω_x is also the frequency at which the root locus crosses the imaginary axis.

An even better separation would consider the particular structure of p_i and p_r so that all the adjustable gains are in Eq. (5b) while Eq. (5a) retains only the overall gain K. In this case, the solution of Eq. (5a) would provide the crossing frequency ω_x as a function of the overall gain K. Once ω_x is substituted into Eq. (5b), the stability boundary can be derived. This is accomplished for a PID controller in the next sub-section.

b) Application to PID Controller

Without delay and nonlinear terms, Eq. (1), as applied to the system of Fig. 1, gives the following controller and spacecraft transfer functions:

$$K \, P(s) = \frac{K_D' s^2 + K_p' s + K_I'}{s^2 + \sigma s + p} \tag{7a}$$

$$D(s) = \frac{1}{s^2} + \sum_{n=1}^{\infty} \frac{k_n}{s^2 + 2\zeta_n \omega_n s + \omega_n^2} \tag{7b}$$

where we have defined:

$$\omega_f \triangleq K_f \triangleq 1/\tau_f$$

$$\sigma \triangleq \omega_f + \omega_m$$

$$\omega_m \triangleq g + 1/\tau_w \qquad (8)$$

$$p \triangleq \omega_f \omega_m$$

$$K_i' \triangleq K_i K_f/I , \qquad i = p, D, I .$$

The flexible modes are written in terms of their unconstrained frequencies ω_n, damping ratios ζ_n and gains k_n. Note that the inertia is found in the control gains rather than in the dynamics transfer function because of its scaling effect on the gains. Following the notation of reference [1] (with one exception), we have, similarly to Eqs. (3):

$$KP(j\omega) = (\gamma + j\delta)/\lambda \qquad (9a)$$

$$D(j\omega) = (\alpha - j\beta) \qquad (9b)$$

with

$$\gamma \triangleq (p-\omega^2)(K_I' - K_D'\omega^2) + K_p'\omega^2\sigma,$$

$$\delta \triangleq \Lambda_{PD}\omega^3 + \Lambda_{PI}\omega,$$

$$\Lambda_{PD} \triangleq \sigma K_D' - K_p'$$

$$\Lambda_{PI} \triangleq p K_p' - \sigma K_I',$$

$$\lambda \triangleq (p-\omega^2)^2 + \sigma^2\omega^2, \qquad (10)$$

$$\alpha \triangleq -\frac{1}{\omega^2} + \sum_{n=1}^{\infty} k_n(\omega_n^2 - \omega^2)/\Delta_n,$$

$$\beta \triangleq 2\omega \sum_{n=1}^{\infty} k_n \zeta_n \omega_n/\Delta_n ,$$

$$\Delta_n \triangleq (\omega_n^2 - \omega^2)^2 + 4\zeta_n^2 \omega_n^2 \omega^2.$$

Note that the control gain K of Eq. (9a) can be taken as K_p' and, consequently, γ/K_p' and δ/K_p' would be functions of the ratios K_D/K_p and K_I/K_p. The CE that corresponds to Eq. (4) is easily obtained as

$$1 + (\alpha\gamma + \beta\delta)/\lambda = 0 \qquad\qquad (11a)$$

$$\alpha\delta = \beta\gamma \qquad\qquad (11b)$$

as shown in Eqs. (27) - (28) of [1]. These equations are modified here following the criteria expressed previously. Equations (5) - (6), as applied to the present problem give:

$$f_{DYN} = -\lambda/\gamma \ ,$$

$$\beta/\alpha = \delta/\gamma \ ,$$

with

$$f_{DYN} \stackrel{\Delta}{=} (\alpha^2 + \beta^2)/\alpha \ .$$

Unfortunately, λ/γ depends on K_I/K_p and K_D/K_p in addition to K_p/I. The separation is not complete so that we must look into the particular structure of γ and δ.

First, note that γ can be rewritten in terms of δ as follows:

$$\gamma = [K_p'\lambda + (\delta/\omega)(\omega^2 - p)]/\sigma \ . \qquad\qquad (12)$$

By substitution, Eq. (11b) can be solved for δ in terms of flexibility parameters:

$$\delta = \frac{(\beta/\alpha) \ K_p'\lambda}{\sigma - (\beta/\alpha\omega)(\omega^2 - p)} \ . \qquad\qquad (13)$$

It is useful to define

$$\delta* = \delta/\omega$$

$$K_p'' = K_p'/\sigma \qquad\qquad (14)$$

$$\Delta = 1 - (\beta/\alpha\omega)(\omega^2 - p)/\sigma$$

so that Eq. (13) can be rewritten as a function of ω^2:

$$\delta* = \frac{(\beta/\alpha\omega) \ K_p''\lambda}{\Delta} \ . \qquad\qquad (15)$$

It is clear that the right-hand side of Eq. (15) depends on the proportional gain while the left-hand side becomes (from Eqs. (10)):

$$\delta* = \Lambda_{PD}\omega^2 + \Lambda_{PI}.$$

After substitution of Λ_{PD}, Λ_{PI} and the ratios:

$$K_D* \triangleq K_D'/K_p" = K_D\sigma/K_p,$$

$$K_I* \triangleq K_I'/K_p" = K_I\sigma/K_p,$$

$$\tag{16}$$

we obtain

$$\delta* = \sigma K_p"\left[(K_D* - 1)\omega^2 + (p - K_I*)\right].\tag{17}$$

Finally, by inserting δ and γ (Eqs. 12-13) into Eq. (11a) one obtains the equation:

$$1 + \alpha(1 + \beta^2/\alpha^2) K_p"/\Delta = 0.\tag{18}$$

At this point, it is useful to define a 'system function' f_{SYS} that is completely independent of the controller gains:

$$f_{SYS} \triangleq \alpha(1 + \beta^2/\alpha^2)/\Delta.\tag{19}$$

Given the wheel dynamics (ω_m), filtering characteristics (ω_f) and the spacecraft dynamics model, f_{SYS} is completely defined and can be plotted versus ω (or ω^2). More will be said later on the interesting properties of f_{SYS}. At this point, we concentrate on the derivation of the stability boundaries from the transformed Eqs. (11):

$$f_{SYS}(\omega) = - 1/K_p"\tag{20a}$$

$$\delta*(\omega) = (\beta/\alpha\omega)K_p"\lambda/\Delta\tag{20b}$$

where $\delta*$ is defined in Eq. (17). We have achieved the separation of the controller and system parameters.

The procedure to obtain the stability boundaries should now be obvious. Once the system function f_{SYS} is plotted versus frequency, a horizontal line is drawn at $-1/K_p"$ for the desired controller gain $K_p"$. As K_p goes from zero to infinity, this horizontal line scans the negative half plane from $-\infty$ to zero. At each intersection of f_{SYS} and $-1/K_p"$, the graph gives the crossing frequency ω_x at which the system goes unstable for that particular gain $K_p"$. Then ω_x is substituted into the right-hand side of Eq. (20b).

to obtain $\delta_x{}^* = \delta^*(\omega_x)$. Finally, from Eq. (17), the relationship between $K_D{}^*$ and $K_I{}^*$ that will allow such a condition is obtained as a straight line of slope ω_x^2 and intercept proportional to $\delta_x{}^*$:

$$K_I{}^* = K_D{}^* \omega_x^2 + (p - \omega_x^2) - \delta_x{}^*/(\sigma K_p{}'') \ . \tag{21}$$

A typical example of this boundary is shown in Figure 2. Analytical results using the Routh Criterion will help interpret these boundaries.

The region of unconditional stability (for all flexibility parameters) that was pointed out in reference [1] can also be recovered from Eqs. (19)–(20). When $\alpha\Delta > 0$, f_{SYS} is always positive and can never intersect the $-1/K_p{}''$ line ($K_p{}'' > 0$): the system is always stable. Since β and λ are positive, $\alpha\Delta > 0$ implies $\delta^* > 0$ from Eq. (20b). Consequently, the combination of $K_D{}^*$ and $K_I{}^*$ in Eq. (17) that will make $\delta^* > 0$ for all frequencies will prohibit any solutions of Eqs. (20) for ω_x and $\delta_x{}^*$. This region of unconditional stability is easily obtained from Eq. (17) as:

$$K_D^* > 1,$$

$$K_I^* < p. \tag{22}$$

The region is shown on Figure 2. These conditions ensure that all roots depart towards the left-hand s-plane and that all asymptotes are also in the LH s-plane. Note that on the stability boundary, $\delta_x{}^* = 0$ for $\zeta = 0$ and $\delta_x{}^* < 0$ when $\zeta \neq 0$.

One may think that all flexible spacecraft stability problems are solved once Eqs. (22) are satisfied by the controller design. In practice, the presence of loop delay and torque limiters drastically alter this 'safe' region. It will be shown that loop delay can easily make a lightly damped flexible mode unstable while saturation elements may shrink this stable region to impractical limits for the rigid mode. The importance of discussing the trivial case (no delay, no limiters) comes from these considerations.

c) Computation and Properties of $f_{SYS}(\omega)$

From its definition, Eq. (19), f_{SYS} depends on ω_m and ω_f through Δ and on the unconstrained modal parameters through α and β. The numerical evaluation of f_{SYS} is thus straightforward, given the system model in unconstrained form. However, these data are often given in constrained form (e.g. by BAe for LSAT in [5]) and a conversion is necessary. From modal identities [4], one can show that:
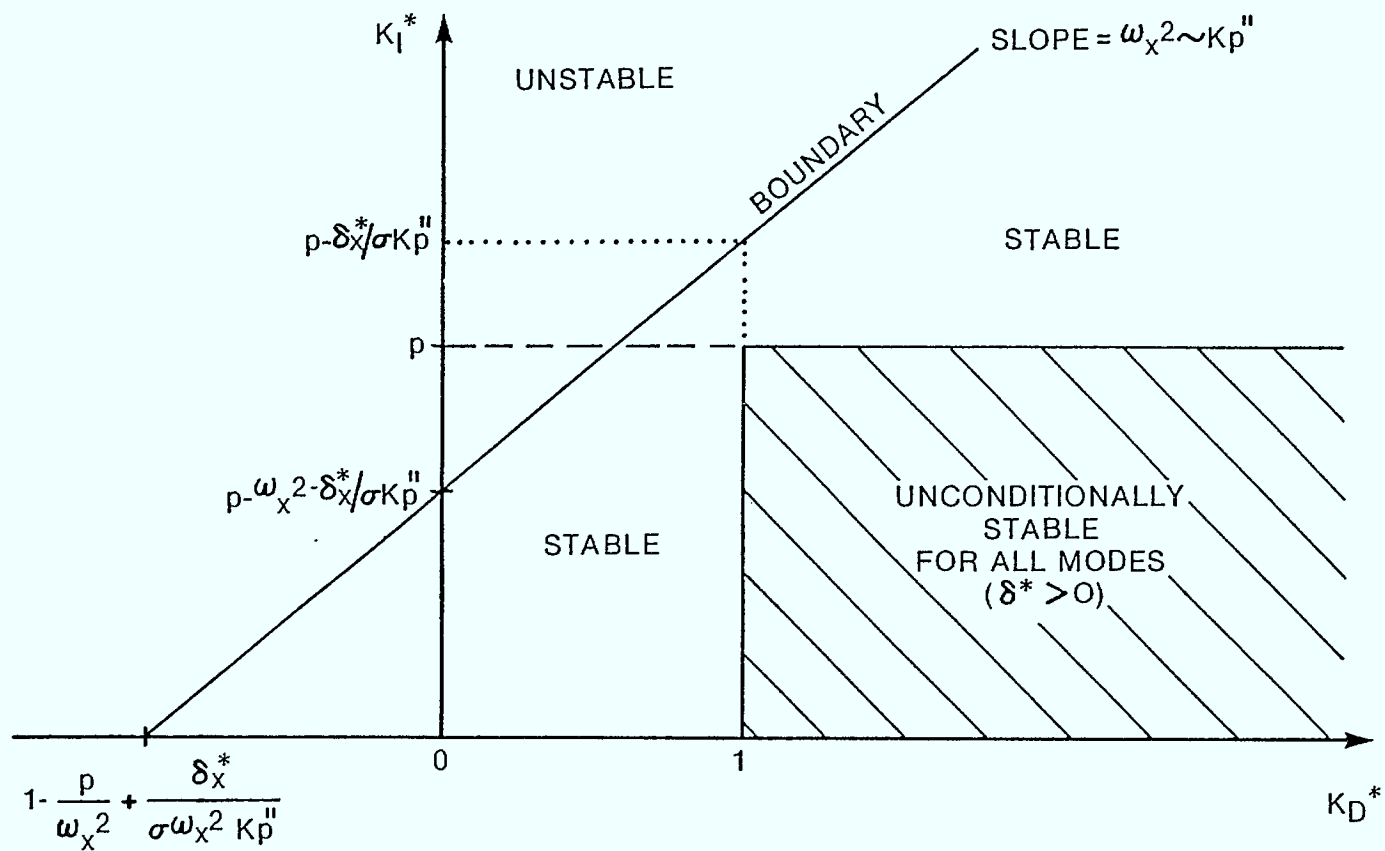
Figure 2   The Stability Diagram For Given $\omega_x{}^2$ and ζ_x^*, ($\zeta_n > 0$).

$$\alpha = - \alpha_c / (\alpha_c^2 + \beta_c^2)$$

$$\beta = + \beta_c / (\alpha_c^2 + \beta_c^2)$$

(23)

where α_c and β_c are the constrained equivalents of α and β:

$$\alpha_c \triangleq \omega^4 \left\{ \frac{1}{\omega^2} + \sum_{n=1}^{\infty} \frac{K_n (\Omega_n^2 - \omega^2)}{(\Omega_n^2 - \omega^2)^2 + 4 Z_n^2 \Omega^2 \omega^2} \right\}$$

(24)

$$\beta_c \triangleq \omega^4 \left\{ 2\omega \sum_{n=1}^{\infty} \frac{K_n Z_n \Omega_n}{(\Omega_n^2 - \omega^2)^2 + 4 Z_n^2 \Omega_n^2 \omega^2} \right\}$$

with K_n, Z_n and Ω_n the constrained modal gains, damping factors and frequencies.

For the undamped case, we have

$$\alpha(\zeta_n = 0) = - \frac{1}{\omega^2} + \sum_n \frac{k_n}{(\omega_n^2 - \omega^2)} \quad ,$$

$$\alpha_c(Z_n = 0) = \omega^4 \left\{ \frac{1}{\omega^2} + \sum_n \frac{K_n}{(\Omega_n^2 - \omega^2)} \right\} \quad ,$$

(25)

$$\beta = \beta_c = 0$$

so that the system function becomes:

$$f_{SYS} = \alpha = -1/\alpha_c, \quad (\zeta = 0).$$

(26)

The above equations present an interesting property of the undamped f_{SYS}:

$$f_{SYS} (\omega = \Omega_n) = 0,$$
$$\qquad\qquad\qquad (\zeta = 0)$$
$$f_{SYS} (\omega \to \omega_n) \to \infty.$$

This is not surprising if one considers that f_{SYS}, Eq. (19), is identical to the dynamics transfer function, Eq. (9b), when there is no damping ($\beta = 0$). Given the constrained modal parameters, f_{SYS} provides a graphical means of obtaining the unconstrained frequencies ω_n. This is much more accurate than the usual one-mode approximation of unconstrained frequencies, $\omega_n \simeq \Omega_n (1-K_n)^{-\frac{1}{2}}$ (as in [5] for instance).

In addition to the evaluation of stability boundaries and unconstrained modal frequencies from constrained modes, f_{SYS} may lead us to another interesting interpretation: the validity of the mode separability assumption.

In the undamped case, the system function is the transfer function between angular acceleration (torque/inertia) and angular displacement; Eqs. (9b) and (19) give

$$f_{SYS} = D(j\omega) = \alpha = \frac{\theta(j\omega)}{T(j\omega)/I} \, , \quad (\zeta = 0).$$

A mode n is said to be separable from the other modes when excitations $T(j\omega)$, with frequencies in a given bandwith B_n around ω_n, produce an output $\theta(j\omega)$ that is mainly character-ized by mode n alone. The contribution of this mode to the transfer function must dominate that of all the other ones. Hence, separability implies:

$$f_{SYS} \simeq \frac{k_n}{(\omega_n{}^2 - \omega^2)} \text{ for } \omega^2 \varepsilon \, B_n, \, \zeta = 0, \tag{27}$$

where $\omega^2 \varepsilon \, B_n$ means $\omega_n{}^2 - B_n/2 \lesssim \omega^2 \lesssim \omega_n{}^2 + B_n/2$. Here, we prefer to express the 'bandwidth' B_n in terms of frequen-cies squared. It is the smallest range of ω^2 within which the magnitude of the one-mode transfer function is larger than some finite and positive value ε. Hence, for $|k_n/(\omega_n{}^2 - \omega^2)| < \varepsilon$ and $\omega^2 \varepsilon \, B_n$, the solution for B_n is

$$B_n = 2k_n/\varepsilon. \tag{28}$$

Since $|k_n/(\omega_n{}^2 - \omega^2)|$ tends to infinity as $\omega \to \omega_n$, it is sufficient to restrict the contribution of the other modes to ε within B_n. The separability criterion takes the form:

$$\max_{\omega^2 \varepsilon \, B_n} \left\{ \left| f_{SYS}(\zeta = 0) - \frac{k_n}{(\omega_n{}^2 - \omega^2)} \right| \right\} < \varepsilon.$$

This is equivalent to the following inequality:

$$\max_{\omega^2 \varepsilon \, B_n} \left\{ \left| \sum_{m \neq n} \frac{k_m}{(\omega_m{}^2 - \omega^2)} \right| \right\} < \varepsilon. \tag{29}$$

In this form, the requirements of small modal gains and large frequency separations are now evident. Note that if $\omega_k{}^2 \, \varepsilon \, B_n$, modes k and n are not separable.

It is clear from Eqs. (28)-(29) that the smaller ε, the more strigent is the condition on separability. For undamped and lightly damped modes, the above criterion is satisfactory with $\varepsilon = 1$. In practice, only a look at the graph of f_{SYS} vs ω gives a relatively accurate assessment of the separability of a given mode, as we shall soon see.

(d) An Example Based on LSAT

Figure 3 shows an undamped, low-frequency sample of f_{SYS} derived from the constrained LSAT roll parameters listed in Appendix 1. The graphical determination of ω_x for a given gain $K_p{}''$ is also illustrated. Note that when $\zeta = 0$, ω_x increases as $K_p{}''$ increases. Due to the sharpness of some of the low-gain modes, the curve does not seem to cross the horizontal axis at Ω_n and go to $\mp \infty$ at ω_n. This aliasing effect is naturally overcome by a smaller plotting interval as shown in Figures 4 and 5 for modes 1 and 3 respectively. A quick glance at Figure 3 reveals a poor separability condition for modes 4 and 5. The same is true, although to a lesser degree, for modes 2 and 3 shown in Figure 6.

Another interesting feature of f_{SYS} is the possibility to analyze the gain stabilization of unstable flexible modes by structural damping or, if insufficient, by flexibility filters. Figures 7-10 illustrate the effect of damping on mode 1 ($\Omega_1 = 0.999$ rad/s). These peculiar transformations of the undamped version already given in Figure 4, come from the fact that the denominator of f_{SYS},

$$\Delta = 1 - (\beta / \alpha \omega) \, (\omega^2 - p) / \sigma \qquad (30)$$

can go through zero since $\zeta \neq 0$ implies $\beta \neq 0$. For small damping, the term $(\beta / \alpha \omega) \, (\omega^2 - p) / \sigma$ has a magnitude greater than unity around ω_n and consequently, Eq. (30) vanishes at two different frequencies as shown in Figures 7-8. Since the $-1/K_p{}''$ line can always intersect f_{SYS}, it is always possible to find a combination of K_D* and K_I* that will define a stability boundary. No matter what $K_p{}''$ is, the system can always be destabilized. As the damping increases towards a critical value given by the solution of
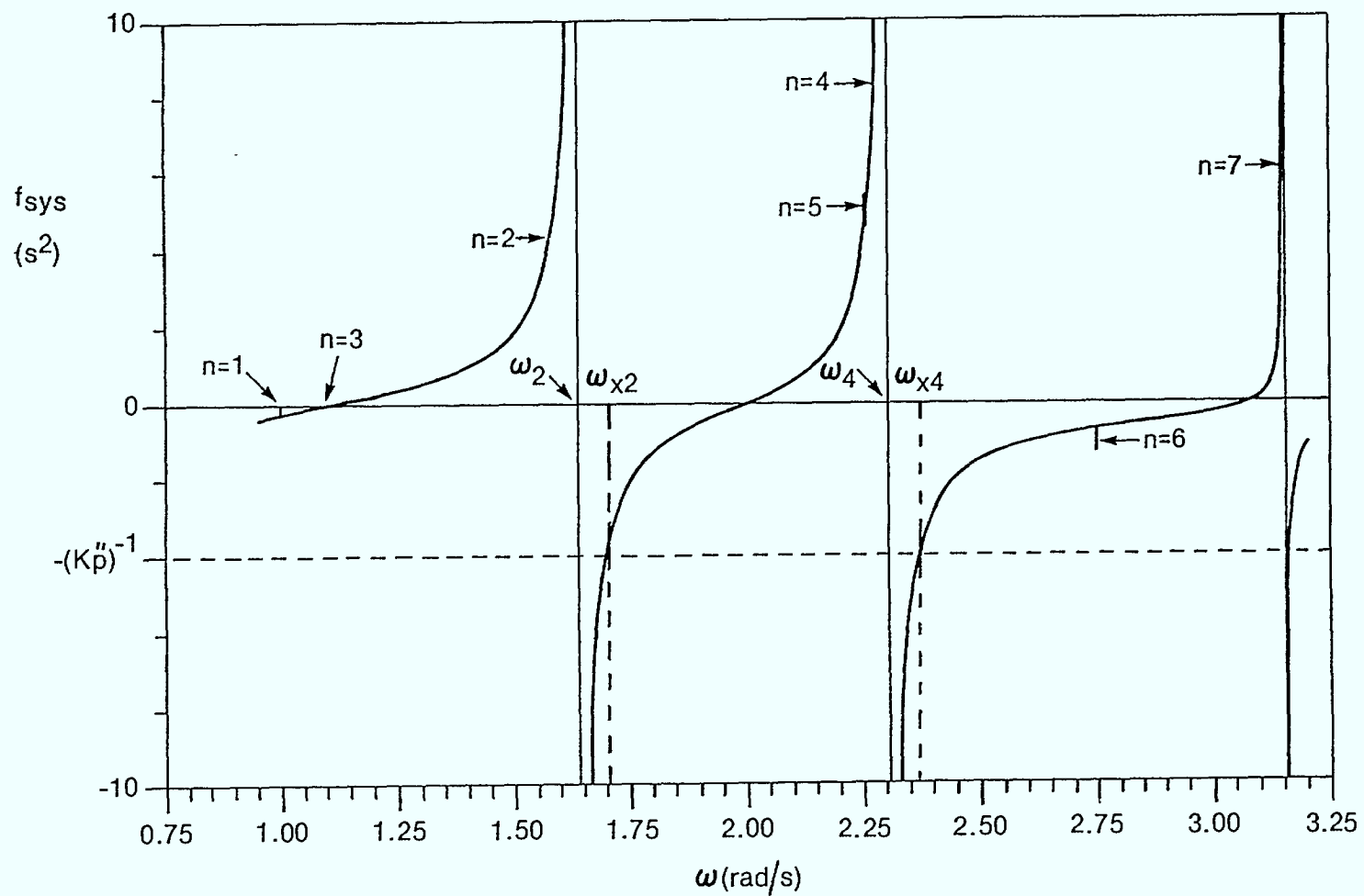
Figure 3   The System Function for LSAT Roll ($\zeta_n = 0$).

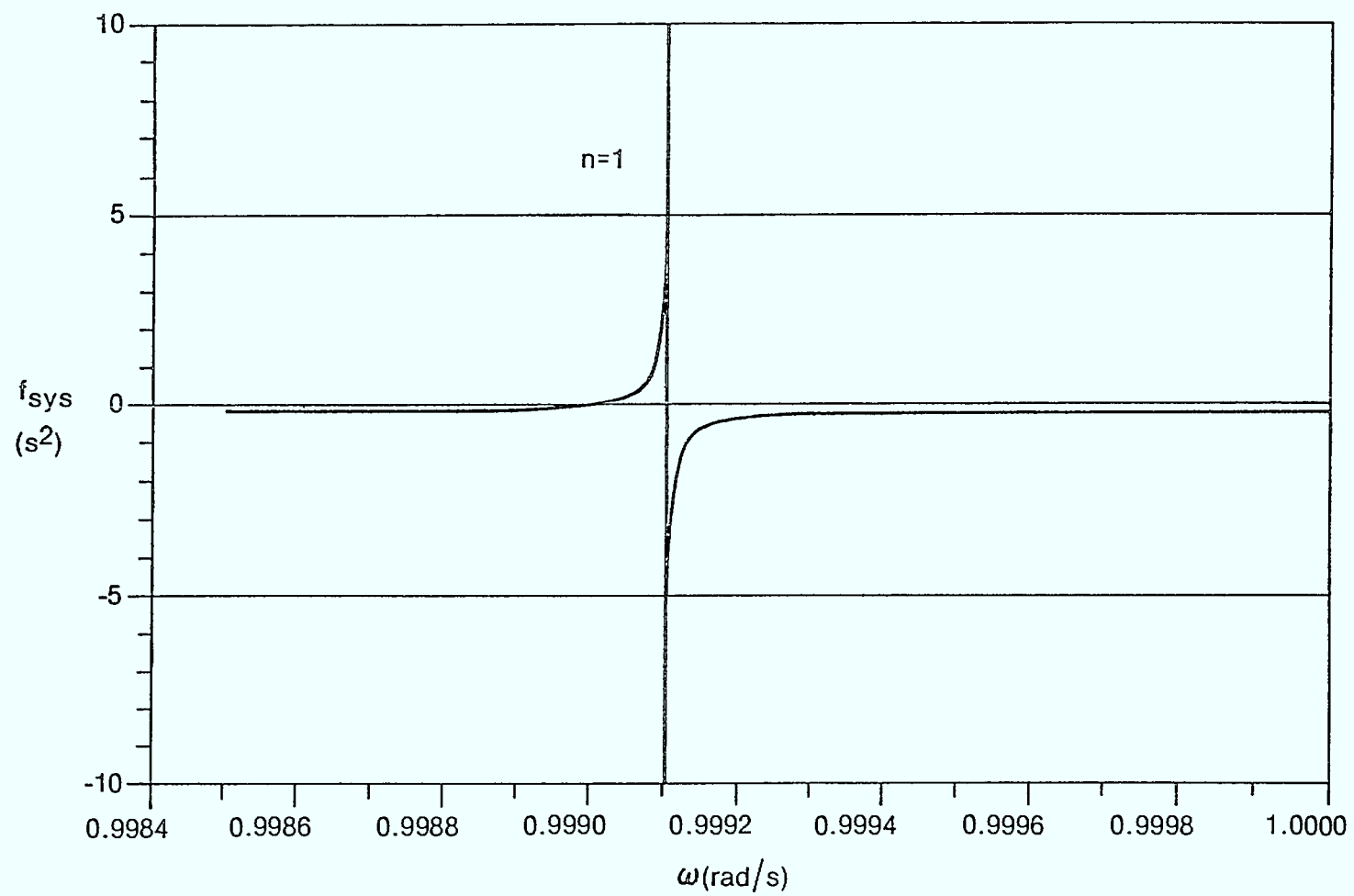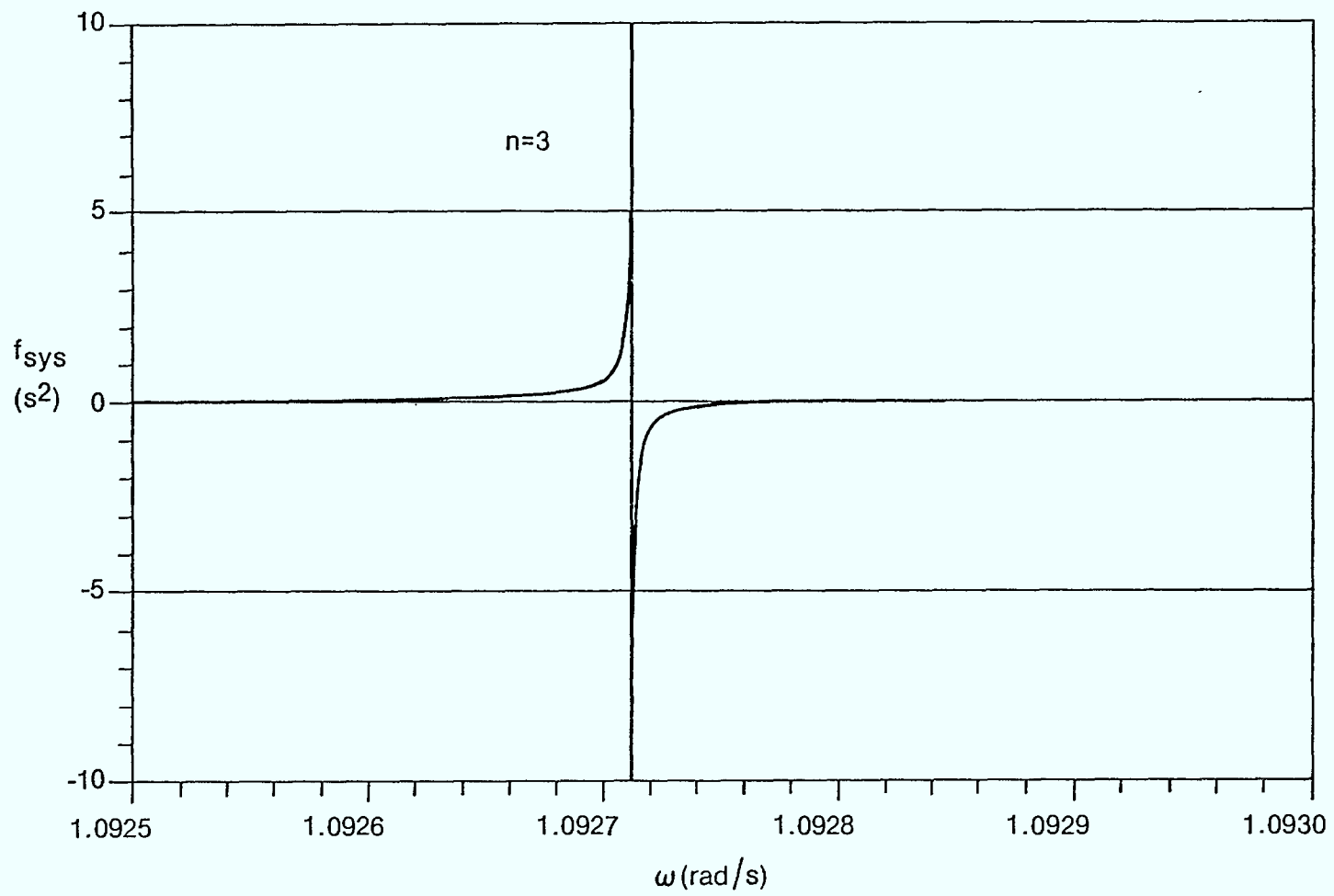Figure 4 Close-up of f_{sys} for Mode 1, $(\zeta_n = 0)$.

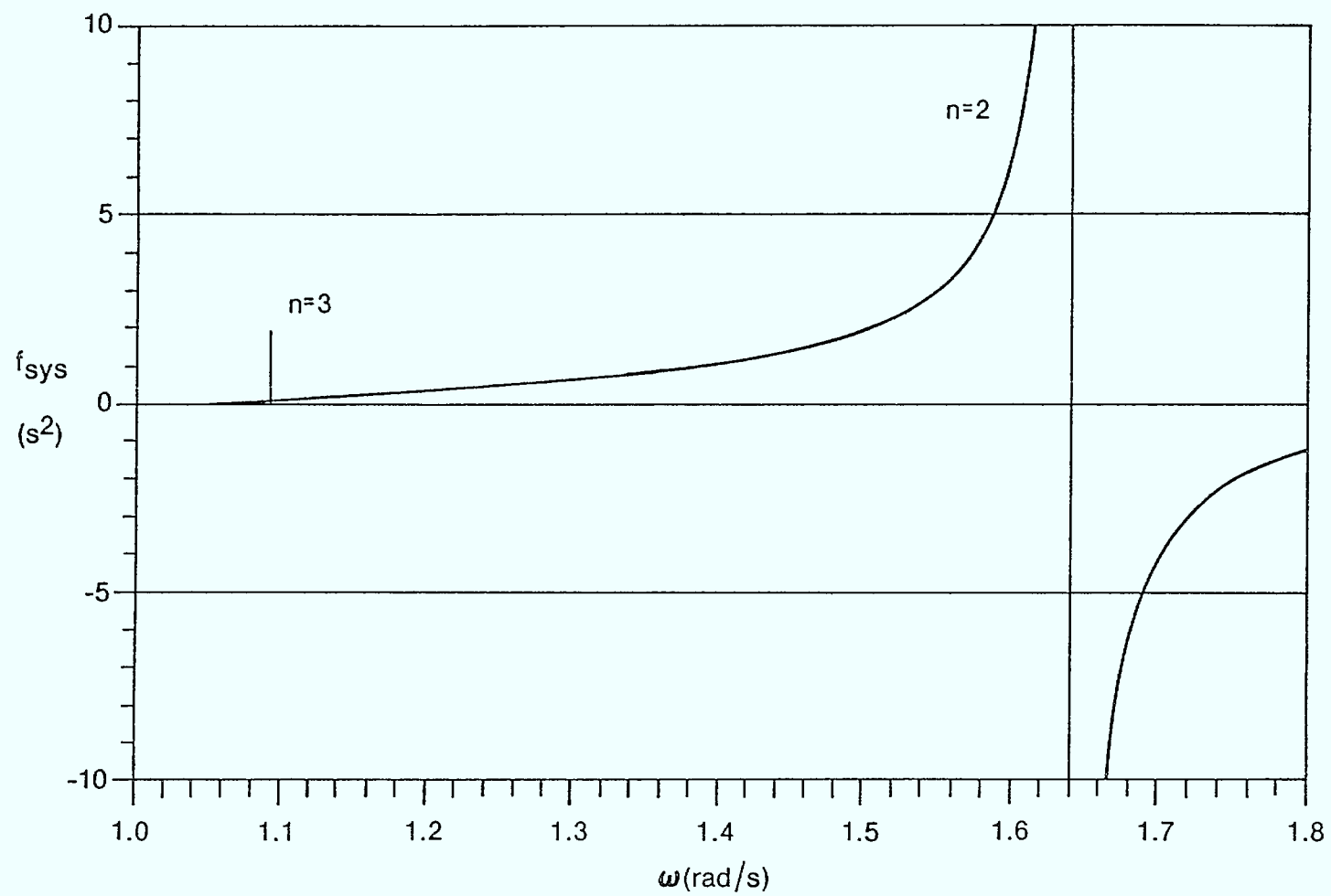Figure 5 Close-up of f_{sys} for Mode 3, $(\zeta_n = 0)$.

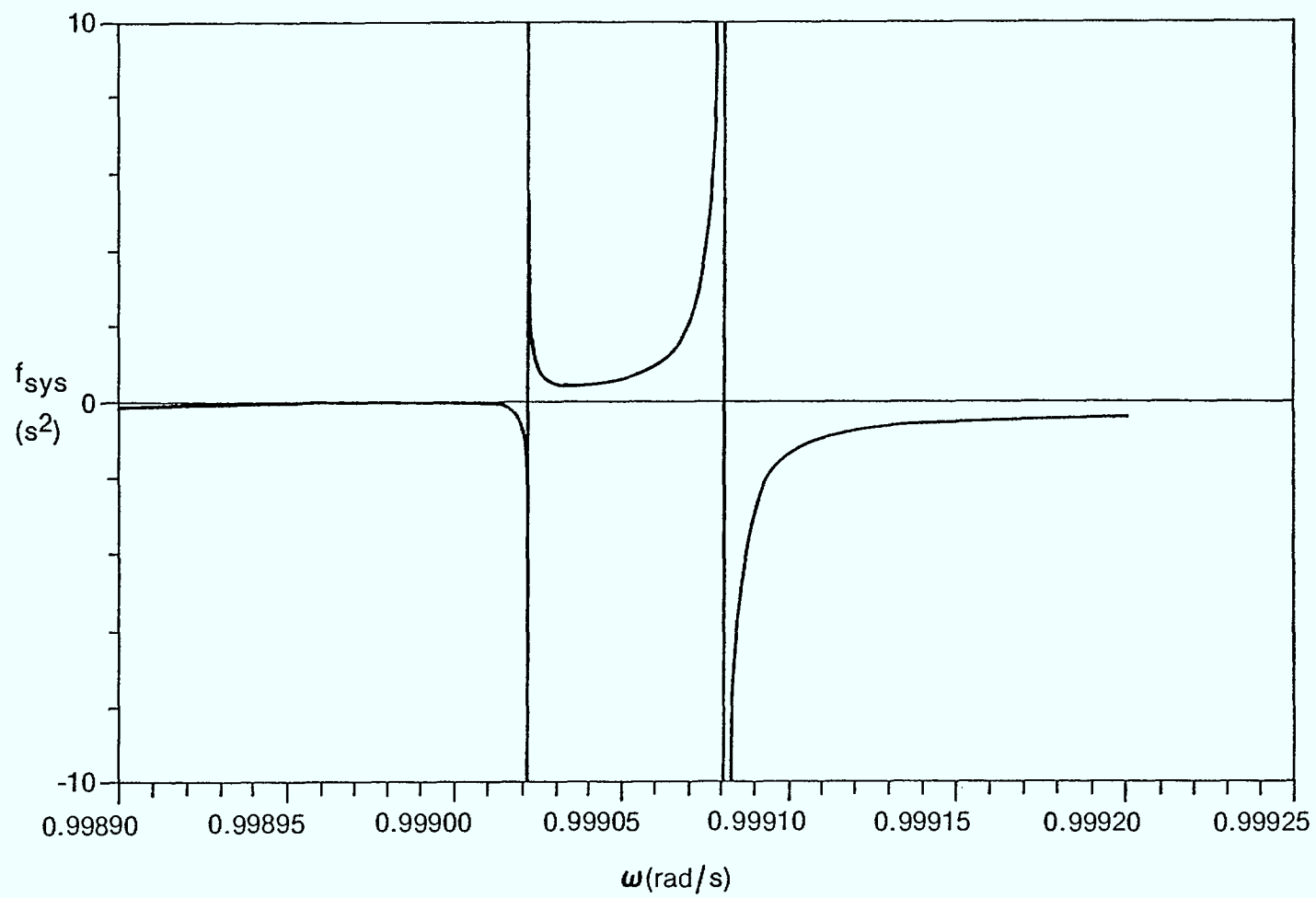Figure 6   Close-up of f_{sys} for Modes 3 and 2 ($\zeta_n = 0$).
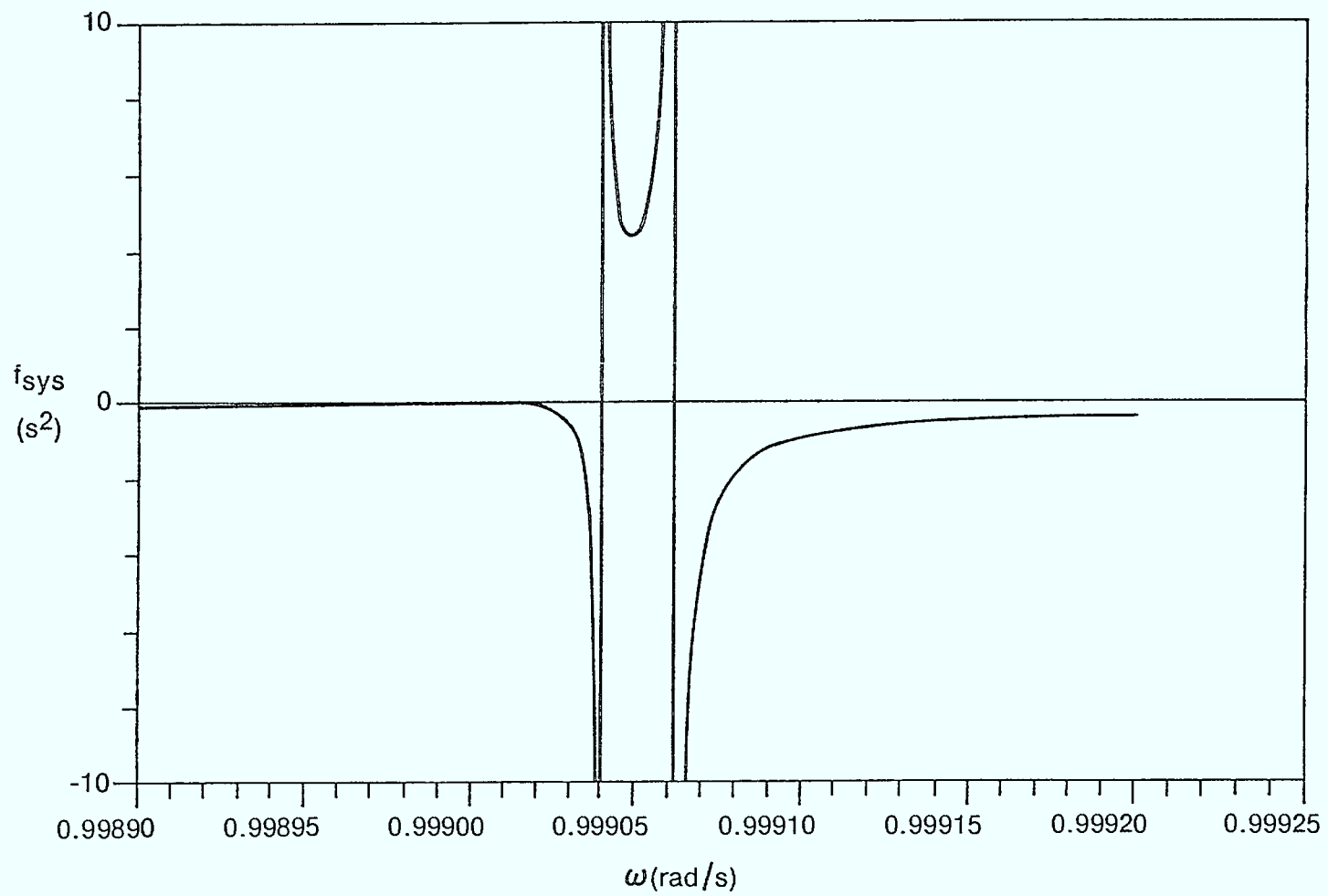
Figure 7 Mode 1 With $\zeta_n = 6 \times 10^{-6}$, n=1,2,...
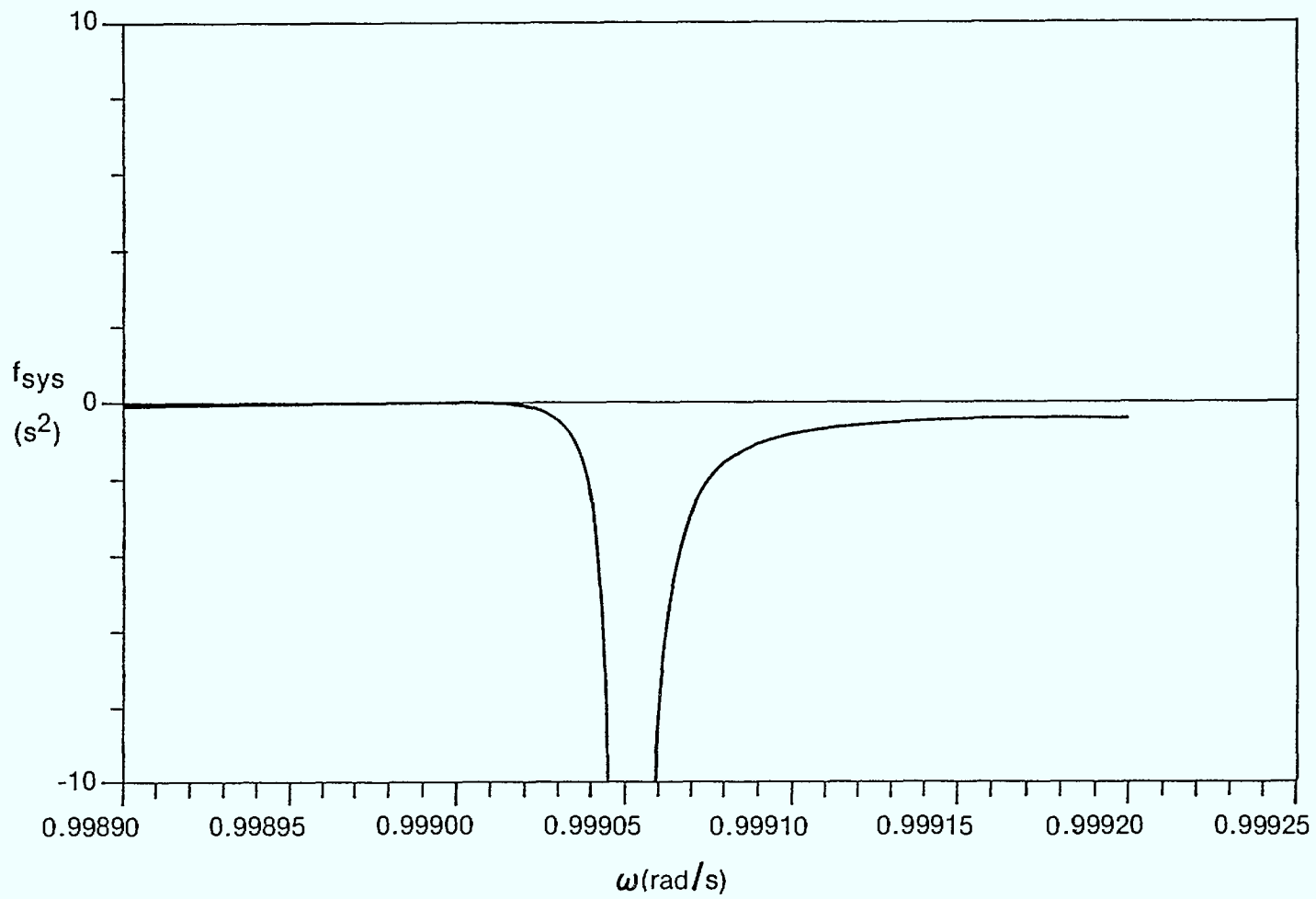
Figure 8   Mode 1 With $\zeta_n = 8.55 \times 10^{-6}$
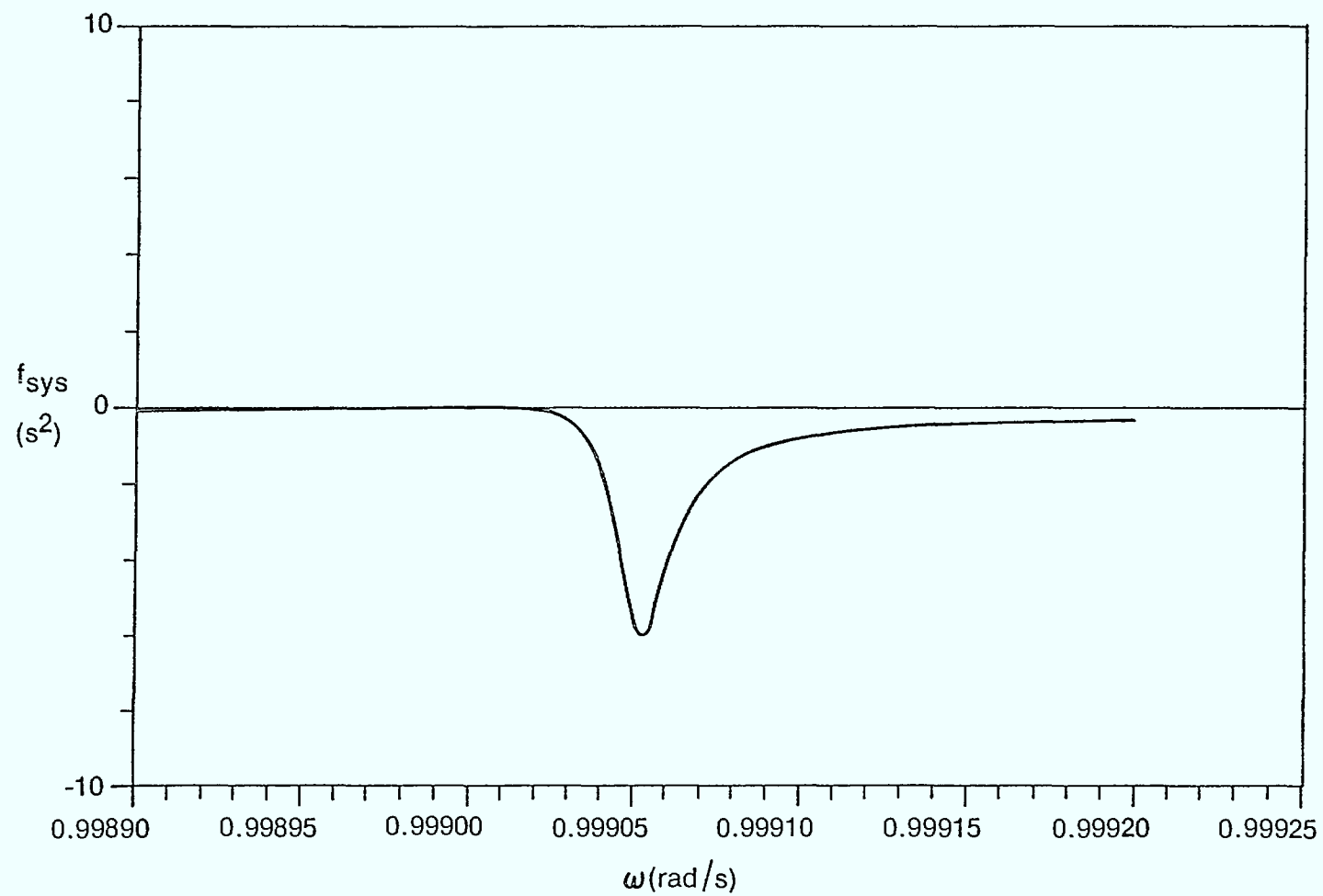
Figure 9   Mode 1 With $\zeta_n = 9 \times 10^{-6}$

Figure 10   Mode 1 With $\varsigma_n = 9.3 \times 10^{-6}$

$$\max_{\omega} \left\{ \left| (\beta/\alpha\omega) (\omega^2-p)/\sigma \right| \right\} = 1, \tag{31}$$

β decreases and eventually brings a unique zero solution for
Equation (30). Only one peak appears, as illustrated in
Figure 9. Above this damping factor, the denominator Δ is
always nonzero and Figure 10 typically results. In this
case, there always exists a maximum controller gain below
which the $-1/K_p{}''$ line can never intersect f_{SYS}. When no
intersection is possible the mode is always stable, no
matter what the values of the positive ratios $K_D{}^*$ and $K_I{}^*$
are; the system can be gain-stabilized by the proper choice
for K_p.

On the other hand, given the gains K_p, K_I and K_D, an
unstable system can also be stabilized by filtering. The
filter break frequency ω_f becomes the variable parameter.
From the definition of $K_p{}''$, Equations (8) and (14), we have

$$K_p{}'' = \frac{K_p}{I} \frac{\omega_f}{\omega_m+\omega_f} \tag{32}$$

and, consequently

$$\lim_{\omega_f \to \infty} (-1/K_p{}'') = -(I/K_p), \tag{33}$$

$$\lim_{\omega_f \to 0} (-1/K_p{}'') = -\infty . \tag{34}$$

Equation (33) corresponds to no filtering at all while Eq.
(34) represents a filter with the smallest possible break
frequency (in practice, ω_f is greater than the controller
bandwidth). The filtering effectively lowers the $-1/K_p{}''$
line and, given a system like Figure 10, an unstable system
may be made stable by a simple decrease in ω_f. These
considerations form the basis of gain stabilization of
flexible modes when there exists a loop delay.

(e) A Comment on the Mode Separability Assumption

In the preceding subsection, it was stated that whenever
the denominator of f_{SYS}, Δ, goes to zero, the $-1/K_p{}''$ line
will always intersect f_{SYS} and instability can always be
induced by a certain combination of $K_D{}^*$ and $K_I{}^*$. This
behaviour could always be avoided by sufficient damping,
making $\Delta \neq 0$ all the time.

Under the assumption of mode separability, the ratio of the modal functions α and β takes the form:

$$\beta/\alpha\omega = \frac{2\zeta_n \omega_n}{(\omega_n^2 - \omega^2)} . \tag{35}$$

This ratio goes to $+\infty$ and $-\infty$ at $\omega=\omega_n$. Substitution of Eq. (35) into Eq. (30) <u>always</u> results in a zero value for Δ at a proper frequency. Hence, mode separability inevitably implies a solution for $f_{SYS} + 1/K_p"=0$ no matter how large ζ_n is; an adequate choice for K_D* and K_I* can always make the system unstable, contrary to the above conclusion. This proves that 'an unstable mode under the separability assumption may in fact be stable when the system as a whole is considered'. This analysis suggests a conservative character for the mode separability assumption. Figures 10 and 11 illustrate the same mode with the same parameters. However, the former includes the first 12 flexible modes (and the rigid mode) while the latter considers one flexible mode only (LSAT roll, n=1). Another observation is the fact that for $K_p"$ large enough, the complete system may be solved for 2 roots ω_x while the one-mode system can only yield one solution at all times. This points out the fundamental difference between each system root locus.

f) Numerical Solution Algorithms

A software package was developed to compute f_{SYS} from constrained or unconstrained modal parameters. A PLOT10 subprogram provides the graphical means for determining ω_x, given $K_p"$. For improved accuracy in the results, a subroutine searches a user-defined range of frequency and monitors f_{SYS} and $df_{SYS}/d\omega$ for sign changes to detect odd-multiple or even-multiple zeros of

$$f_{SYS} + 1/K_p" = 0. \tag{36}$$

After detection, a Newton-Raphson algorithm is automatically initiated for convergence to the desired zero, in this case ω_x^2. Analytical approximations, derived in the next section, are also computed to provide the user with initial estimates useful in the numerical solution algorithm. However, as these closed-form results are based on the separability assumption, the graphical output of f_{SYS} must also be consulted in case a solution for (36) disappears as a result of modes interaction.
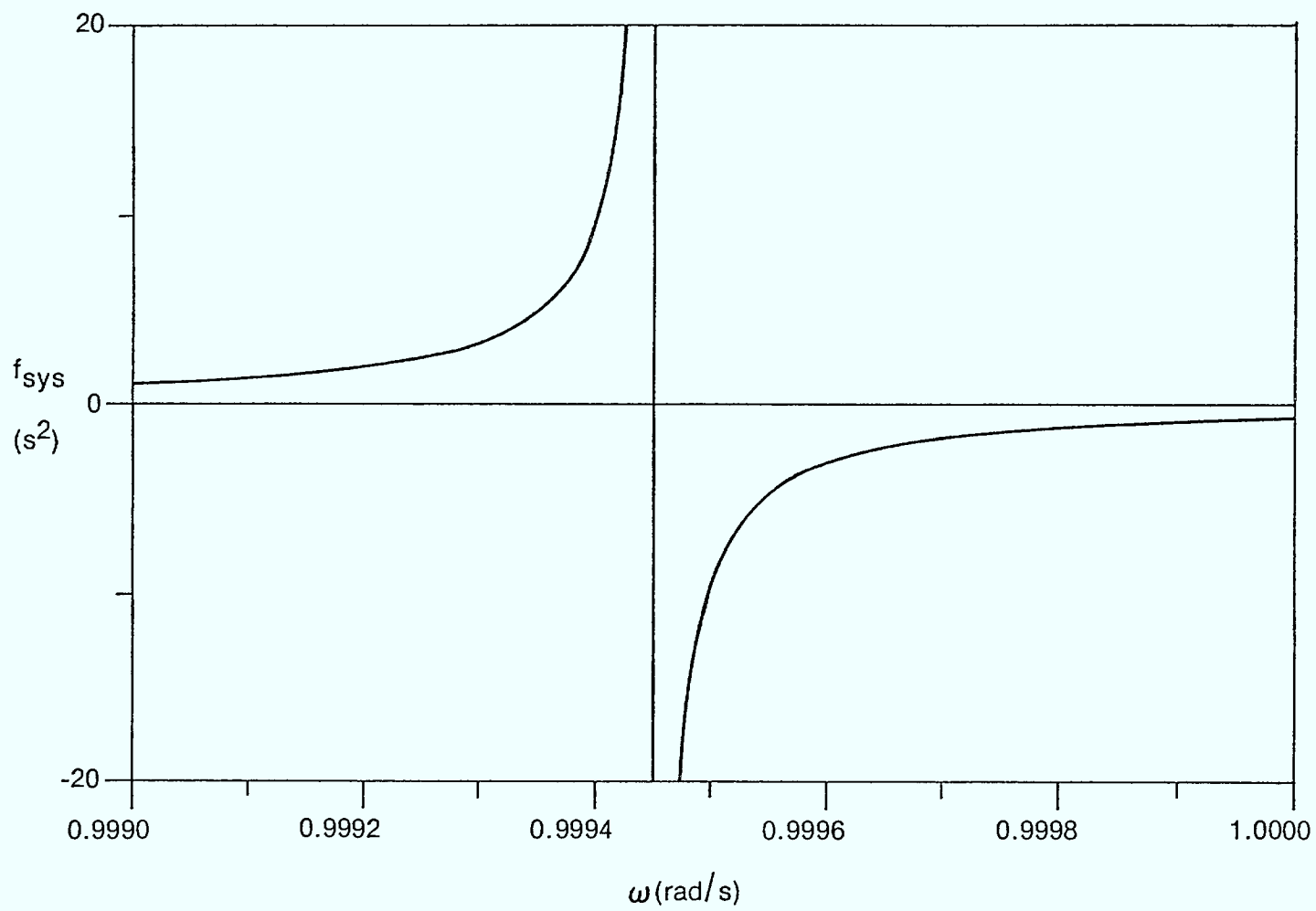
Figure 11   'Separated' Mode 1 With $\zeta_1 = 9.3 \times 10^{-6}$

4. Analytic Derivation of the Boundary Equations

This section will first repeat the final results of reference [2] as a background to the presentation of a more complete analysis. These observations will support the interpretation of the numerical approach discussed in Section 3.

(a) Method and General Form

As observed earlier, the analytical results are made possible with the introduction of an additional assumption, that of mode separability. Under this condition, the spacecraft dynamics are simplified as follows:

$$D(s) = \frac{k_n}{s^2 + 2\zeta_n \omega_n s + \omega_n^2} , \qquad n=0,1,2\ldots \qquad (37)$$

with n=0 representing the rigid mode ($k_0=1$, $\omega_0=0$). The linear controller of Figure 1 without delay has the form

$$P(s) = \frac{K_D's^2 + K_p's + K_I'}{s^2 + \sigma s + p} \qquad (38)$$

and the characteristic equation is thus completely described. The application of the Routh Stability Criterion to this system gives the following condition for stability (Eq. 8 of [2] rewritten in a different form):

$$K_I^* < K_D^* \omega_x^2 + (p-\omega_x^2) - \delta_x^*/(K_p''\sigma) \qquad (39)$$

where

$$\omega_x^2 = (\omega_n^2 + k_n K_p'' + pz_n/\sigma)/(1 + z_n/\sigma), \qquad (40)$$

$$z_n = 2\zeta_n \omega_n, \qquad (41)$$

$$\delta_x^* = - \frac{z_n}{k_n} \left[(\omega_x^2-p)^2 + \sigma^2 \omega_x^2 \right] . \qquad (42)$$

Note that the above results are consistent with the boundary given by Eq. (21) once α and β are modified according to the separability assumption and substituted into Eqs. (20). This time however, we have approximate closed-form relations for ω_x and δ_x^*.

For every mode, inequality (39) defines a stable region in the $K_D{}^* - K_I{}^*$ plane with $K_p{}''$ as a parameter. The boundary is a straight line of slope $\omega_x{}^2$. Note that Eq. (42) is in accordance with an earlier comment (Section 3): $\delta_x{}^*$ is negative or zero on the stability boundary depending on whether there is structural damping or not. By rewriting Eq. (39) as

$$(K_D{}^* - 1) \, \omega_x^2 + (p - K_I{}^*) > \delta_x{}^* / (K_p{}'' \, \sigma)$$

and noting that $\delta_x{}^* \leq 0$, the system is unconditionally stable whenever $K_D{}^* > 1$ and $K_I{}^* < p$, as we showed in Eq. (22).

The implications of Eq. (39) and Eq. (21) are best understood by consideration of simple cases.

(b) Analysis of Particular Cases
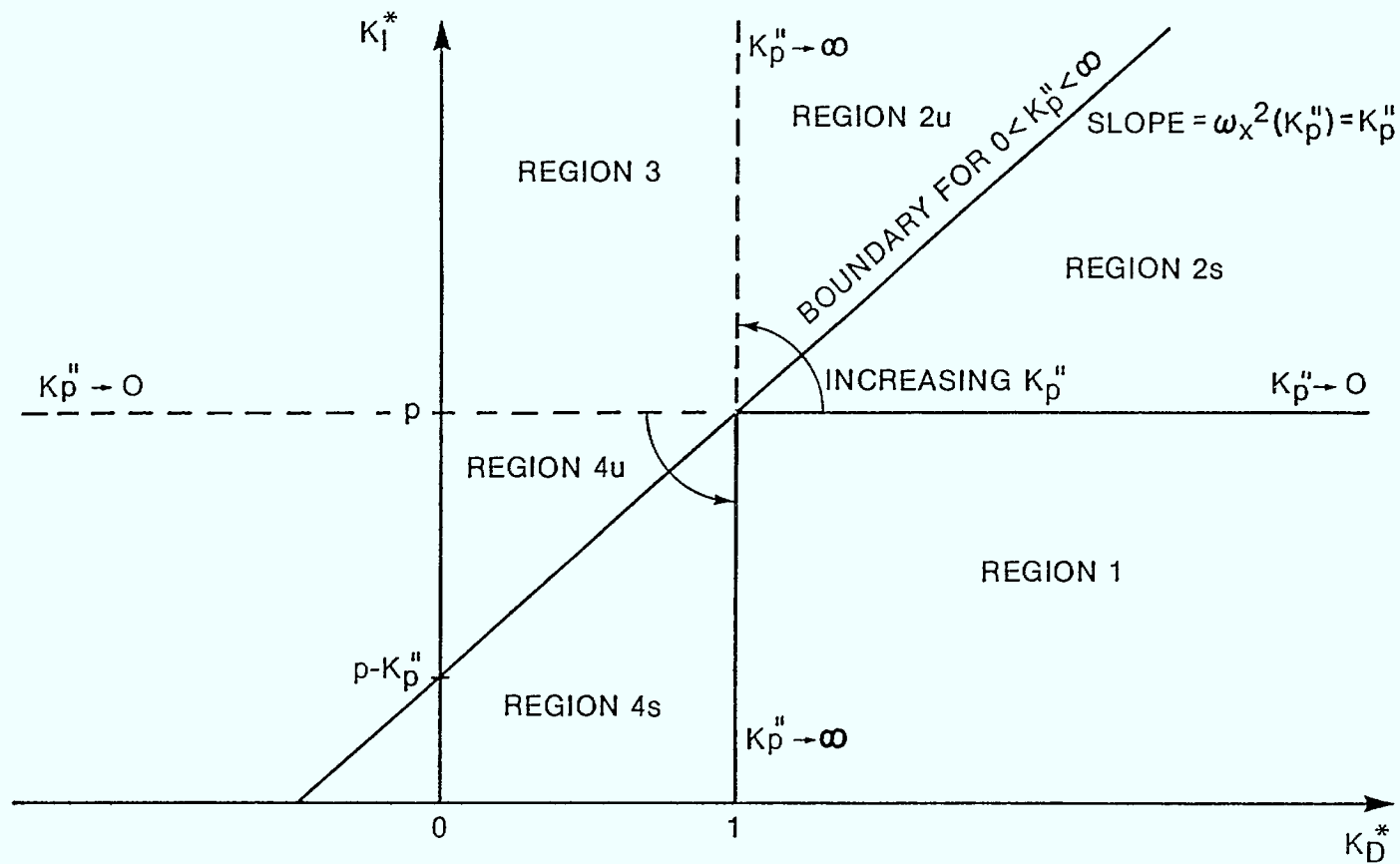
For the rigid mode, we have

$$K_I{}^* < K_D{}^* \, K_p{}'' + (p - K_p{}'') \tag{43}$$

because $\omega_x{}^2 = K_p{}''$ and $\delta_x{}^* = 0$. The boundary is a horizontal line through $K_I{}^* = p$ for $K_p{}'' = 0$ and becomes a vertical line at $K_D{}^* = 1$ for $K_p{}'' \to \infty$. The counter-clockwise rotation of the boundary occurs around the point $(1,p)$ as shown in Fig. 12. In this figure, the regions of unconditional and conditional stability have been identified for future reference.

For an undamped flexible mode, Eq. (39) reduces to:

$$K_I{}^* < K_D{}^* \, (\omega_n^2 + k_n K_p{}'') + (p - \omega^2 - k_n K_p{}'') \tag{44}$$

This time, the slope starts at $\omega_n{}^2$ but the rotation is still about the same point. When the flexible mode frequencies are outside the controller bandwidth ($\omega_n{}^2 > K_p{}''$), the stability diagram takes the form of Figure 13. Note that the region of unconditional stability for mode n contains that for the rigid mode. Hence, for all the spacecraft modes, the intersection of these regions is that for the rigid mode, i.e. Eq. (22).

Figure 12 Stability Diagram for the Rigid Mode

REGION 1   : UNCONDITIONALLY STABLE
REGIONS 2,4 : CONDITIONALLY STABLE (s = stable)
REGION 3   : UNCONDITIONALLY UNSTABLE

Figure 13 Stability Diagram for an Undamped Flexible Mode n

(c) Analysis of the General Case

For a damped flexible mode, the slope of the boundary increases with K_p''. However, it does not touch the region of unconditional stability anymore: damping moves the boundary up (Fig. 2). While it is straightforward to obtain the boundary for a given K_p'', it is not easy to visualize how it moves with varying K_p''. This is due to the fact that no fixed point - like the (1,p) rotation point of the undamped cases - can be defined. The results of [2] are here extended in order to shed some light on this general case.

Inserting Eqs. (40)- (42) into (39), we obtain a condition in term of a parabolic dependence on K_p'', symbolized here by the function $F(K_p'')$:

$$F(K_p'') = a_n K_p''^2 + b_n K_p'' + c_n > 0 \tag{45}$$

where

$$a_n \triangleq k_n^2 [(\sigma + z_n)(K_D^* - 1) + z_n],$$

$$b_n \triangleq k_n \{(\sigma + z_n)(\omega_n^2 + z_n p/\sigma)(K_D^* - 1) + (\sigma + z_n)^2 (p - K_I^*)/\sigma$$

$$+ z_n [\sigma(\sigma + z_n) + 2(\omega_n^2 - p)]\},$$

$$c_n \triangleq z_n [(\omega_n^2 - p)^2 + (\sigma + z_n)(\sigma \omega_n^2 + p z_n)].$$

Because of Eq. (45) and since $K_p'' > 0$, a graph of $F(K_p'')$ versus K_p'' will determine a stable system whenever the locus is in the first quadrant.

In particular, the undamped system would have

$$F'(K_p'') = a_n' K_p'' + b_n' > 0, \tag{46}$$

with

$$a_n' = k_n(K_D^* - 1),$$

$$b_n' = \omega_n^2(K_D^* - 1) + (p - K_I^*). \tag{47}$$

Equation (46) is plotted in Figure 14 for various combinations of K_D* and K_I*. The system is always stable when $a_n' > 0$, $b_n' > 0$ (Region 1) and always unstable when $a_n' < 0$, $b_n' < 0$ (Region 3). Conditional stability, (depending on K_p''), exists when $a_n' > 0$, $b_n' < 0$ (Region 2) or $a_n' < 0$, $b_n' > 0$ (Region 4). These different curves are associated to Figures 12-13 by their region number. The system unconditional stability region, Eq. (22), (Region 1 for the rigid mode) is easily recovered from Eq. (47) by setting $a_0' > 0$, $b_0' > 0$.

In the damped case, Eq. (45) applies and parabolas are obtained as shown in Fig. 15. The correspondence with the previous case is the same as far as Region numbers are concerned. The difference is that, since $c_n > 0$, the system always starts stable at $K_p'' = 0$. Therefore, Region 3, in addition to 2 and 4, becomes conditionally stable. For a large enough damping ratio, we may have

$$b_n^2 < 4a_n c_n \tag{48}$$

and part of Region 2 may become unconditionally stable. For Region 1, where $a_n > 0$, $b_n > 0$, we have the following relationship for unconditional stability:

$$K_D* > 1 - \frac{z_n}{(\sigma + z_n)}$$

$$\tag{49}$$

$$K_I* < p + \frac{(\sigma \omega_n^2 + p z_n)}{(\sigma + z_n)} (K_D* - 1) + \frac{z_n}{(\sigma + z_n)} \left[\sigma^2 + 2\sigma \frac{(\omega_n^2 - p)}{(\sigma + z_n)} \right].$$

It is obvious that these limits, plotted in Figure 16, contain those for the undamped case. It can now be concluded that, as K_p'' increases from zero, the boundary moves down from $+\infty$ on the K_I* axis. The slope of the boundary increases with K_p'' while the intercept decreases. As $K_p'' \to \infty$, the slope and the intercept go to infinity at $K_D* = 1 - z_n/(\sigma + z_n)$. In this process, some points in Region 2 become unstable and stable again while some others are always on the stable side. The curve (arc of an eclipse) separating these points is found by solving $b_n^2 = 4a_n c_n$. Region 1 of Figure 16 is thus a conservative region of unconditional stability.

In terms of a root-locus diagram, it can also be concluded that when $b_n < 0$, the locus departs toward the right-half s-plane: instability occurs at $K_p'' = 0$ ($\zeta = 0$) or near it ($\zeta > 0$). For $a_n < 0$, an asymptote of the locus is in the right-hand s-plane, and the system becomes and remains unstable as K_p'' increases toward infinity.
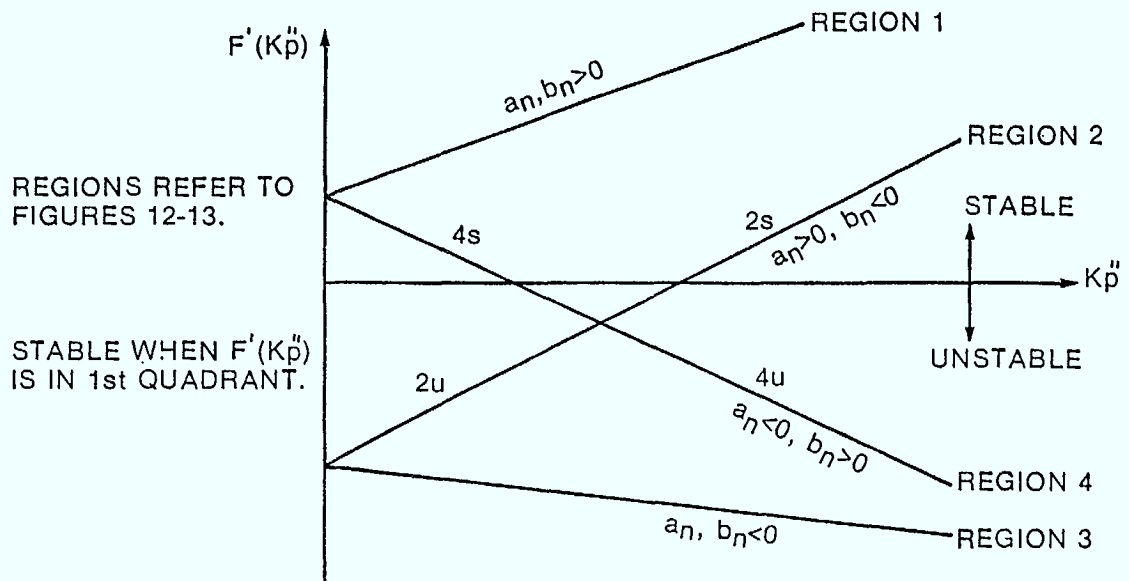
Figure 14 Graphs of F' vs Kp"
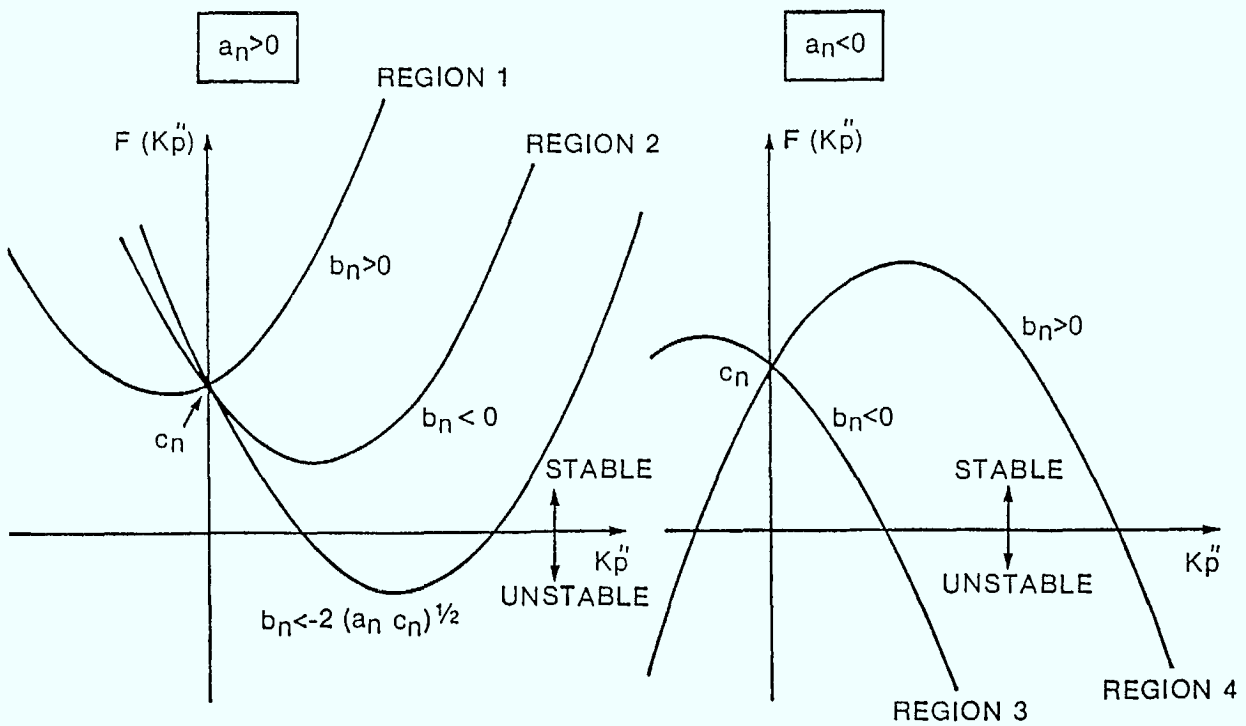
Figure 15 Graphs of F vs Kp"
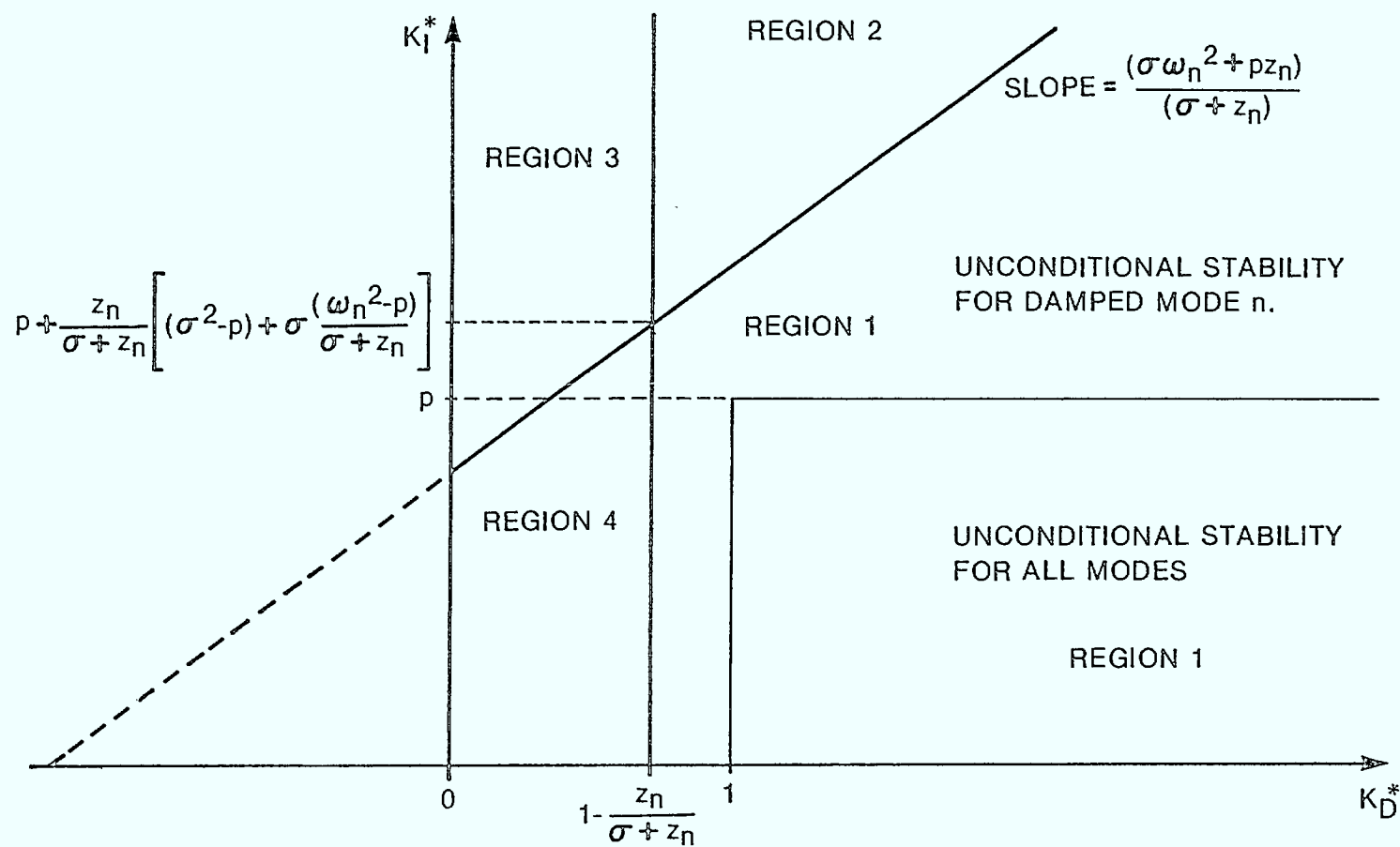
Figure 16 Stability Diagram for the Damped Flexible Mode n.

d) Comments

The above approximate results help to interpret the stability diagram of Figure 2 which was obtained from a numerical solution for the fundamental parameters ω_x and $\delta_x{}^*$. It should be remembered however that mode separability is assumed in the analytics. Section 3(e) has warned us that for a given K_p'', a solution for ω_x may not exist for a given mode due to interaction from other modes. Equation (40), limited by the assumption, can yield a solution ω_x for all K_p''. A more detailed analysis of this effect would probably conclude that the boundary of Figure 16 is, in fact, more conservative than the actual case.

5. Delay and Nonlinear Effects

The tools that have just been implemented were tried on a simple system for illustration purposes. The extension to more complex systems is usually straight-forward; the basic principles implied by f_{SYS}, ω_x^2 and δ_x^* still apply. The addition of loop delay does not preclude the definition of f_{SYS} while nonlinear elements can be accommodated by the describing function approach. The only complication is in the increased number of parameters (delay T, equivalent gain k_L); the interpretation of the results is not a trivial exercise.

It is not the purpose of this study to present a detailed analysis of delay and nonlinear effects. This was carried out in [2] and [6] respectively. We will rather complement these analyses in the context of system function and stability diagrams.

(a) Loop Delay

In reference [2], the delay factor was approximated by:

$$e^{-Ts} \simeq T_0 + T_1 s, \tag{50}$$

with

$$T_0 = \cos\omega_n T,$$

$$T_1 = -\sin\omega_n T/\omega_n,$$

$$T = \text{delay}.$$

In the context of mode separability, this form allowed the 'tuning' of the delay term to any modal frequency ω_n $n=0,1,2,...$ so that accurate gain and phase result at ω_n. In the same reference, the integral term was chosen so that it cancelled the wheel dynamics. One must set $K_I = \omega_m = 0$ in the present model for correspondance with that in [2]. Combining Eq. (50), mode separability and Routh Criterion, it was then possible to derive the so-called critical frequencies ω_c:

$$\omega_{ck} = \frac{k\pi}{T} \frac{(1+\omega_f T)}{(1+\frac{1}{2}\omega_f T)} + \left[\frac{k^2\pi^2}{T^2\left(1+\frac{1}{2}\omega_f T\right)^2} + \frac{\omega_f}{T\left(1+\frac{1}{2}\omega_f T\right)} \right]^{\frac{1}{2}}, \tag{51}$$

$$k=0,1,2...$$

The 0th order critical frequency:

$$\omega_{co} = \left[\frac{\omega_f}{T\left(1 + \frac{1}{2}\omega_f T\right)} \right]^{\frac{1}{2}} \tag{52}$$

is in accordance with Eq. (33) of [3]. A mode n with its frequency in the range $\omega_{ck} < \omega_n < (k2\pi + \pi/2)/T$ is shown to be unstable unless there exists damping to allow gain stabilization.

The complexity of this approach required $K_I = \omega_m = 0$ and mode separability. The present method can thus complement it with more general results. Using the identity $e^{-j\omega T} = \cos\omega T - j\sin\omega T$, the equations defining the stability boundaries become

$$f_{SYS} = (-1/K_p") \cos\omega T \tag{53a}$$

$$\delta* = (M/\omega)\lambda K_p"/\Delta_T \tag{53b}$$

with the system function defined as:

$$f_{SYS} \triangleq \alpha(1 + M\beta/\alpha)/\Delta_T \tag{54}$$

and

$$\Delta_T \triangleq 1 - (M/\omega)(\omega^2 - p)/\sigma, \tag{55}$$

$$M(\omega) \triangleq \frac{\alpha\sin\omega T + \beta\cos\omega T}{\alpha\cos\omega T - \beta\sin\omega T}. \tag{56}$$

When T=0, $M(\omega)$ and Δ_T reduce to β/α and Δ respectively; Eqs. (20) are recovered. Note that from Eq. (53a), the intersection of f_{SYS} is not with a straight line anymore but a cosine function of amplitude $-(K_p")^{-1}$.

As usual, the stability diagram inferred by Eqs. (53)-(56) is best understood by consideration of the undamped modes. With $\zeta_n = 0$, n=1,2,..., we get

$$\beta = 0,$$

$$M(\omega) = \tan\omega T,$$

$$\Delta_T = 1 - (\tan\omega T/\omega)(\omega^2 - p)/\sigma, \tag{57}$$

$$f_{SYS}(\zeta_n = 0) = \alpha/\Delta_T.$$

Note that f_{SYS} is the same as in the undelayed case, Eq. (25), except that it is now divided by Δ_T. The properties of this denominator will be shown to be of great importance below.

Figures 17 and 18 show the graphs of f_{SYS} with exactly the same parameters used in Figure 3 except that delays of T=0.1s and T=0.2s have been included. In the undamped case, we have proved that f_{SYS} goes to $\mp \infty$ at every unconstrained frequency ω_n. This is still verified in Figures 17 - 18. However, comparison with Figure 3 reveals that an additional infinite peak has been introduced by the nonzero delay. This new pole, located at the critical frequency ω_{co}, is evidently accounted for by Δ_T. On Figures 17-18, the reader may verify that Δ_T (dashed line) goes through zero at precisely ω_{co}. Consequently, for $\omega < \omega_{co}$, f_{SYS} is not substantially altered by a delay ($\Delta_T > 0$) but it is inverted for $\omega > \omega_{co}$ as it is multiplied by a negative number ($\Delta_T < 0$).

The critical frequency ω_{co} is the solution of $\Delta_T = 0$. By assuming ωT small, a closed-form approximate equation for ω_{co} is:

$$\omega_{co} \simeq \left\{ \frac{\sigma + pT}{T(1 + \frac{1}{2}\sigma T)} \right\}^{\frac{1}{2}} . \tag{58}$$

Using the parameters of Appendix 1, Eq. (58) gives

$$\omega_{co}(T=0.2s) \simeq 1.318 \text{ rad/s},$$

$$\omega_{co}(T=0.1s) \simeq 1.873 \text{ rad/s},$$

in accordance with the exact numerical result shown in Figures 17-18. Furthermore, if we let $\omega_m = 0$ in Eq. (58) (i.e. $\sigma = \omega_f$ and p=0), the particular cases treated in [2] and [3] are recovered as Eq. (52). The kth critical frequency ω_{ck} can also be derived from Eq. (58) by assuming $\omega T - k2\pi$ small (k=0,1,2,...) and a result similar to Eq. (51) is easily obtained.

Now that the properties of f_{SYS} are known, we investigate the stability region it defines. Inserting Eqs. (57) into Eqs. (53)-(56), we get:

$$f_{SYS} = \alpha/\Delta_T = -(K_p")^{-1} \cos \omega T, \tag{59a}$$

$$(\zeta = 0)$$

$$\delta^* = (\tan \omega T / \omega) \lambda K_p" / \Delta_T . \tag{59b}$$
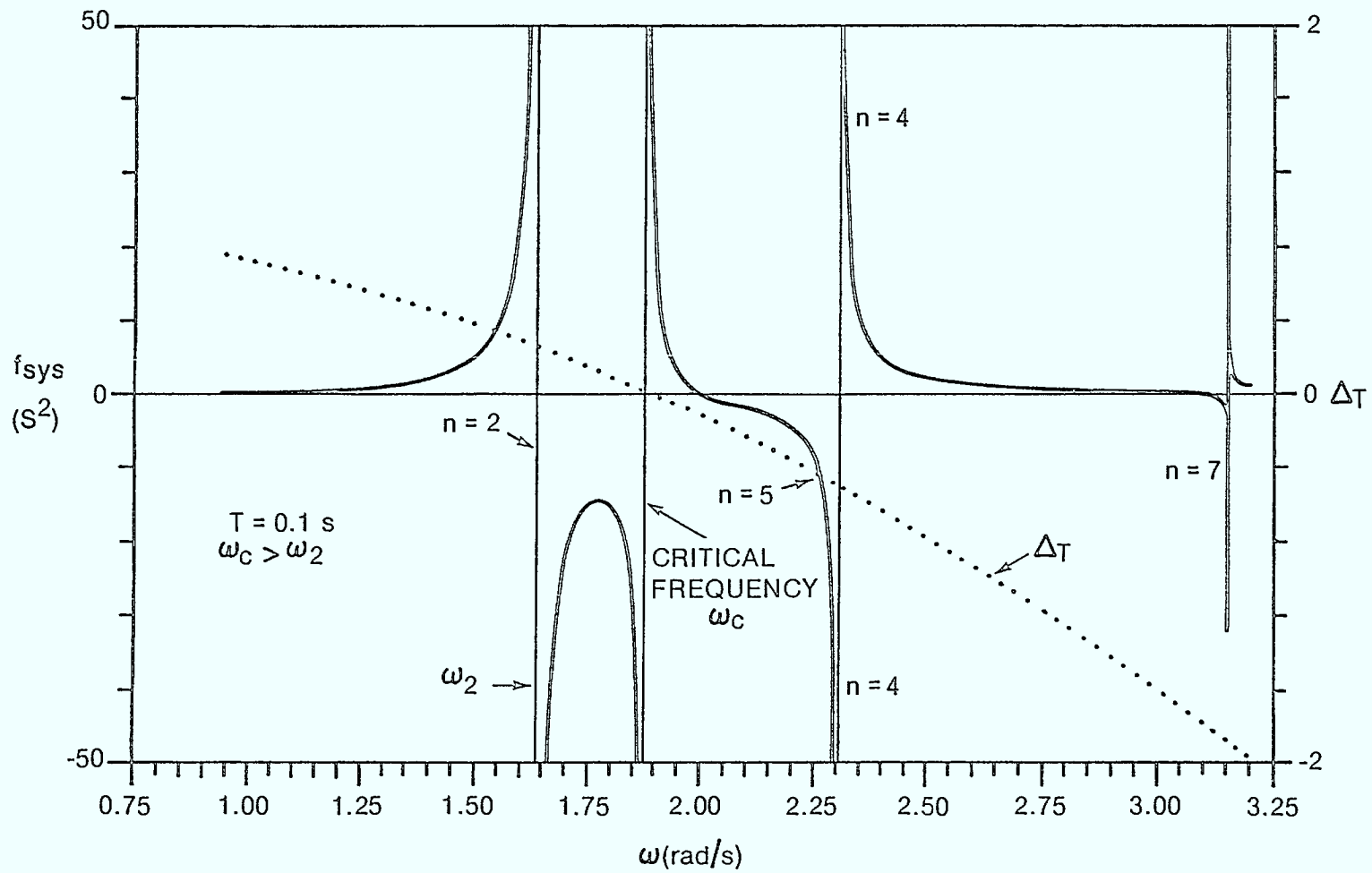
Figure 17(a)   The System Function and Δ_T for LSAT Roll With Delay T = 0.1 s
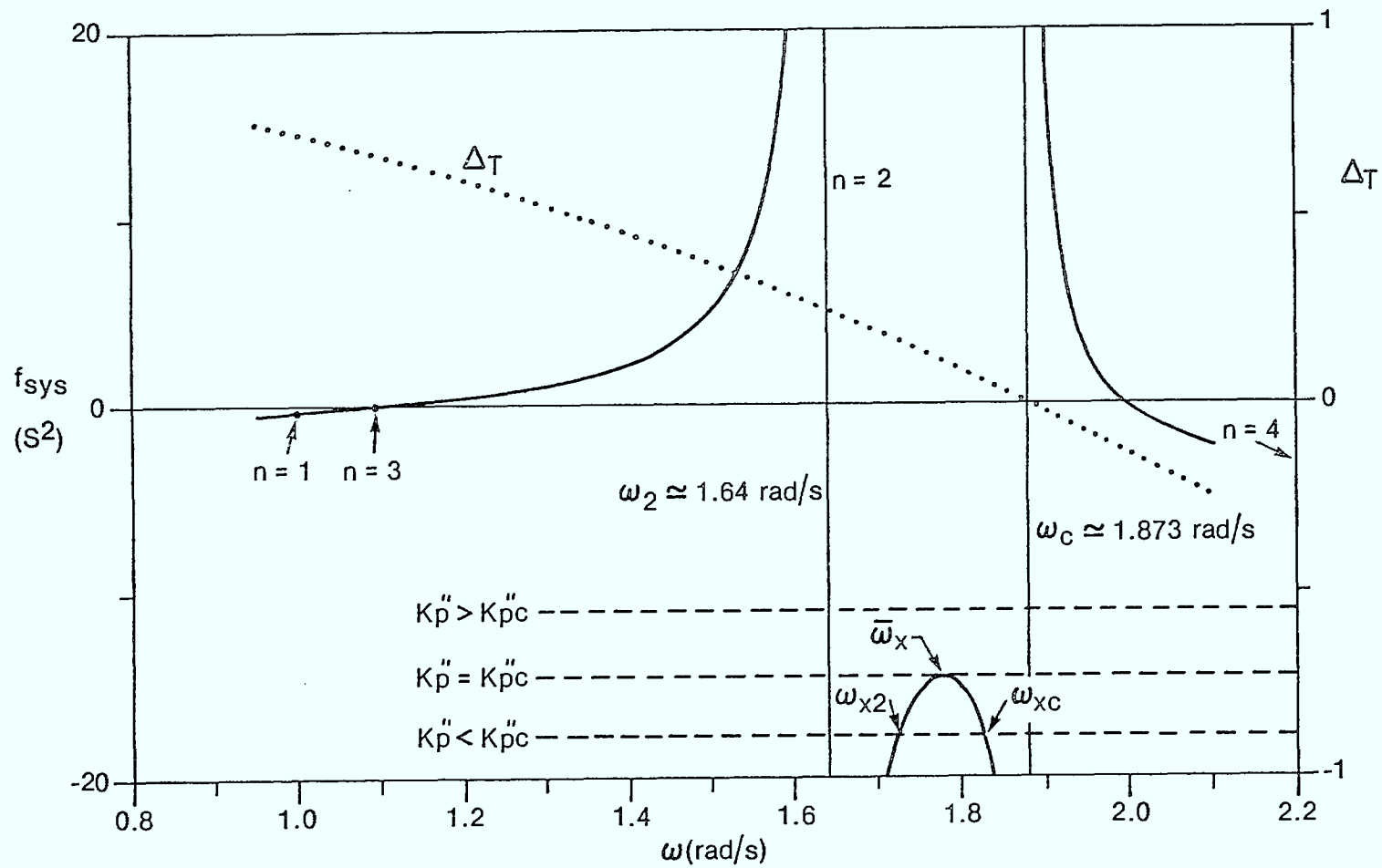
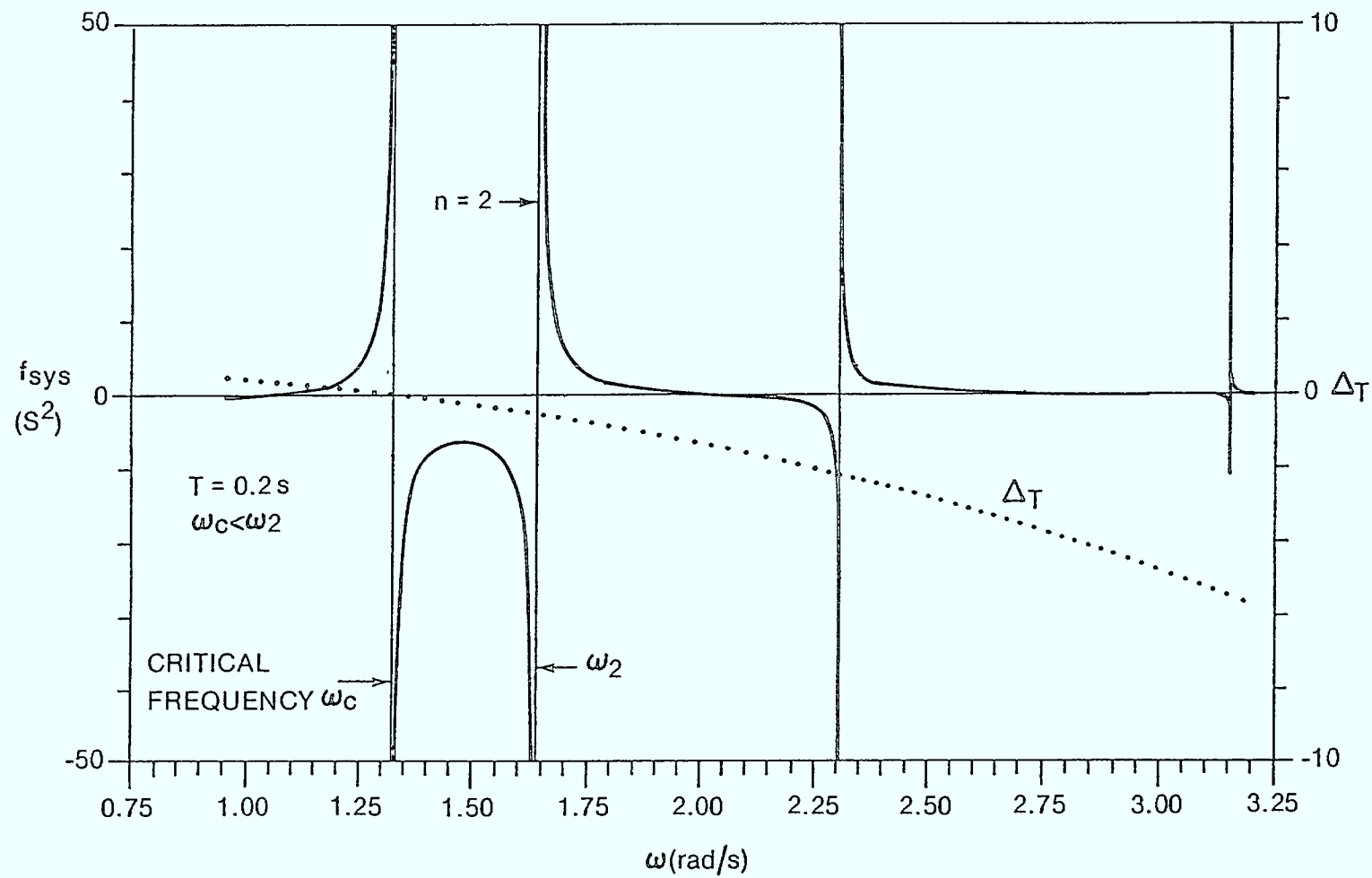Figure 17(b)   Close-up of Fig. 17(a) Near ω_a and ω_c

Figure 18(a)   The System Function and Δ_T for LSAT Roll With Delay T = 0.2 s
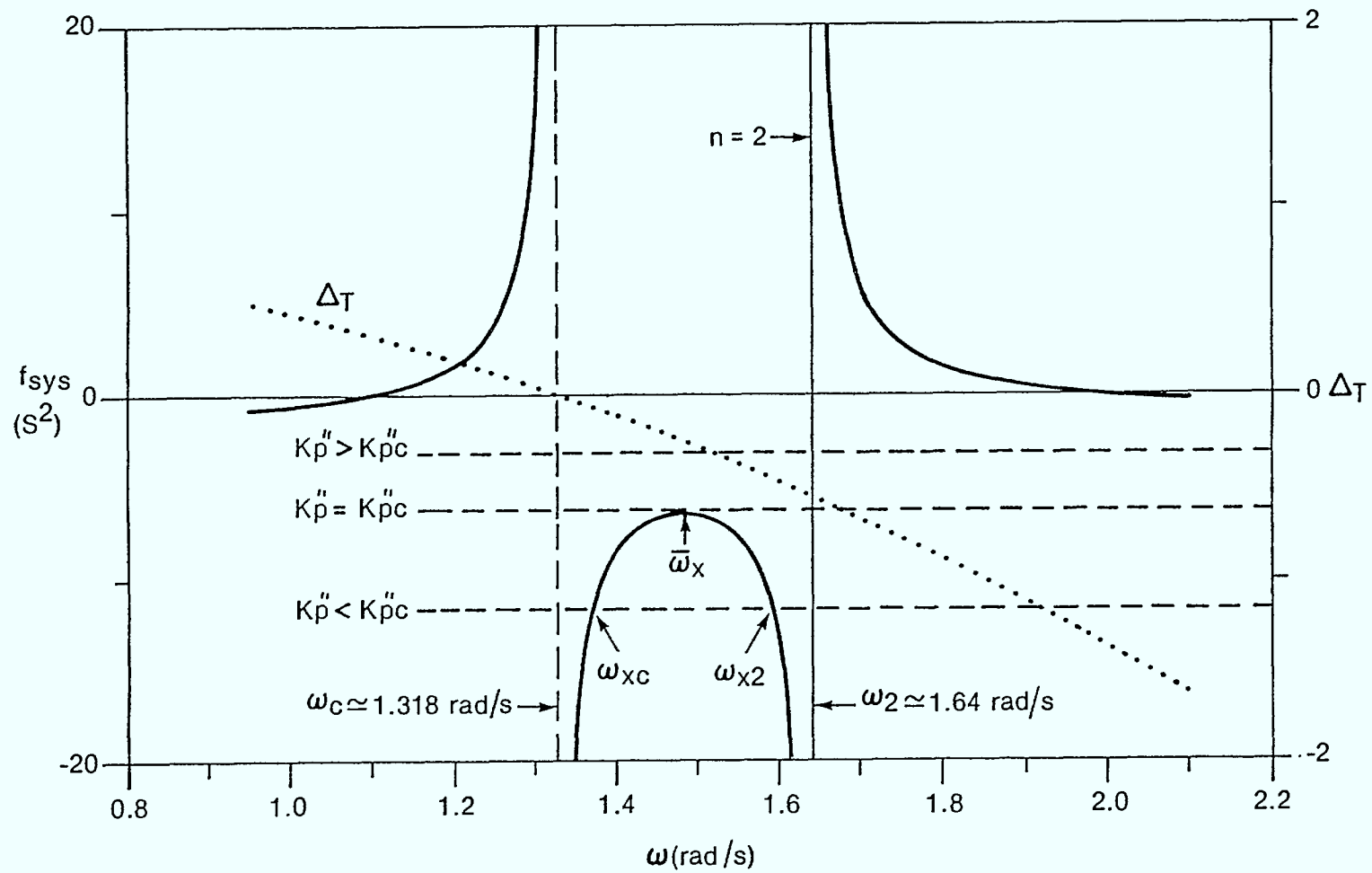
Figure 18(b) Close-up of Fig. 18(a) Near ω_2 and ω_c

For T=0, we have shown that Eq. (59a) could be solved for with an infinite number of solutions ω_{xn}^2, n=0,1,2,... such that $\omega_{xn}^2 > \omega_n^2$: see Figure 3. With T≠0, the presence of Δ_T brings a new solution at ω_{xc}^2 near ω_c^2. The system stable region in the K_D^* - K_I^* plane becomes the intersection of the stable regions defined by all these boundaries.

For the present analysis, we will concentrate on the frequency range $0 \leqslant \omega T \leqslant \pi/2$. This interval contains all the modes of interest for most spacecraft (for T=0.2s, $0 \leqslant \omega \leqslant$ 7.85 rad/s) and is the only interval where the modes can be phase unstable, as proved in [2]. The discussion considers the mode n closest to the critical frequency ω_c (n=2 in Figures 17-18). The extension of the results to other modes is trivial.

The reader is referred to Figs. (17b) and (18b) for the following analysis. Near ω_c and ω_n, an approximate solution to Eq. (59a) is:

$$\omega_{xn}^2 = \overline{\omega}_x^2 + f \, W_{\frac{1}{2}} \qquad\qquad (60a)$$

$$\omega_{xc}^2 = \overline{\omega}_x^2 - f \, W_{\frac{1}{2}} \qquad\qquad (60b)$$

with

$$\overline{\omega}_x^2 \overset{\Delta}{=} \tfrac{1}{2}(\omega_n^2 + \omega_c^2) \qquad\qquad (61)$$

$$W_{\frac{1}{2}} \overset{\Delta}{=} \tfrac{1}{2}(\omega_n^2 - \omega_c^2)$$

and f is a positive fraction, which is a function of the gain:

$$f \overset{\Delta}{=} \left\{ 1 - \frac{K_p'' \, k_n \sigma}{T \, W_{\frac{1}{2}}^2 \, \cos\omega_n T} \right\}^{\frac{1}{2}}. \qquad\qquad (62)$$

When K_p'' =0, we have f=1 and the roots are $\omega_{xn}^2 = \omega_n^2$ and $\omega_{xc}^2 = \omega_c^2$. As K_p'' increases, both ω_{xn}^2 and ω_{xc}^2 tend to $\overline{\omega}_x^2$ until they both coincide when f=0 at a value of K_p'' called the critical gain K_{pc}'':

$$K_{pc}'' \approx T \, W_{\frac{1}{2}}^2 \, \cos\omega_n T/(k_n \sigma) . \qquad\qquad (63)$$

As $K_p"$ is further increased, no real solution exists for Eq. (59a). The graphical equivalent of these results is illustrated in Figures (17b)-(18b). In the vicinity of ω_c and ω_n, ω_{xn}^2 and ω_{xc}^2 are the squares of the frequencies at which f_{SYS} intersects the curve $(-K_p")^{-1} \cos\omega T \approx (-K_p")^{-1} \cos\omega_n T$. This curve moves from $-\infty$ to zero as $K_p"$ increases from 0 to ∞.

Now let us consider the case when $\omega_2 < \omega_c$ (Figure 17b). We then have $(0 < K_p" < \infty)$:

(i) $\qquad \omega_n^2 < \omega_{xn}^2 < \underset{(n=2)}{\bar{\omega}_x^2} < \omega_{xc}^2 < \omega_c^2$, $\qquad\qquad$ (64)

(ii) $\qquad \Delta_T \geqslant 0$ at ω_2, $\qquad\qquad\qquad\qquad\qquad\qquad$ (65)

(iii) $\qquad 0 < \delta_{xn}^* < \delta_{xc}^* < \infty$. $\qquad\qquad\qquad\qquad\qquad$ (66)

The parameter $\delta_{xn}^*(\delta_{xc}^*)$ is Eq. (59b) evaluated at ω_{xn}^2 (ω_{xc}^2). From Figure 2, the boundary associated with ω_{xn}^2 has an increasing slope (from ω_n^2 to $\bar{\omega}_x^2$) and a decreasing intercept ($\sim -\delta_{xn}^*$). The boundary associated with ω_{xc}^2 starts from $K_I^* = -\infty$ (intercept $\sim -\delta_{xc}^* \sim -\infty$) at a slope of ω_c^2 and moves upward with a decreasing slope ω_{xc}^2. The stable region is below the ω_{xn}^2 line and above the ω_{xc}^2 line. At $K_p" = K_{pc}"$, the two lines coincide at a slope $\omega_{xc}^2 = \omega_{xn}^2 = \bar{\omega}_x^2$ ($\delta_x^* = \delta^*(\bar{\omega}_x^2)$) and the system is unstable everywhere. Figure 19 depicts the stability diagram of mode 2 (LSAT Roll) with $T=0.1$s (so that $\omega_2 < \omega_c$). Stability requires $K_p" < K_{pc}"$.

When $T=0.2$s, we have $\omega_2 > \omega_c$ (Figure 18) and for $0 < K_p" < \infty$:

(i) $\qquad \omega_c^2 < \omega_{xc}^2 < \bar{\omega}_x^2 < \omega_{xn}^2 < \omega_n^2$, $\qquad\qquad$ (67)

$\qquad\qquad\qquad\qquad\qquad (n=2)$

(ii) $\qquad \Delta_T \leqslant 0$ at ω_2, $\qquad\qquad\qquad\qquad\qquad\qquad$ (68)

(iii) $\qquad -\infty < \delta_{xc}^* < \delta_{xn}^* < 0$. $\qquad\qquad\qquad\qquad\qquad$ (69)
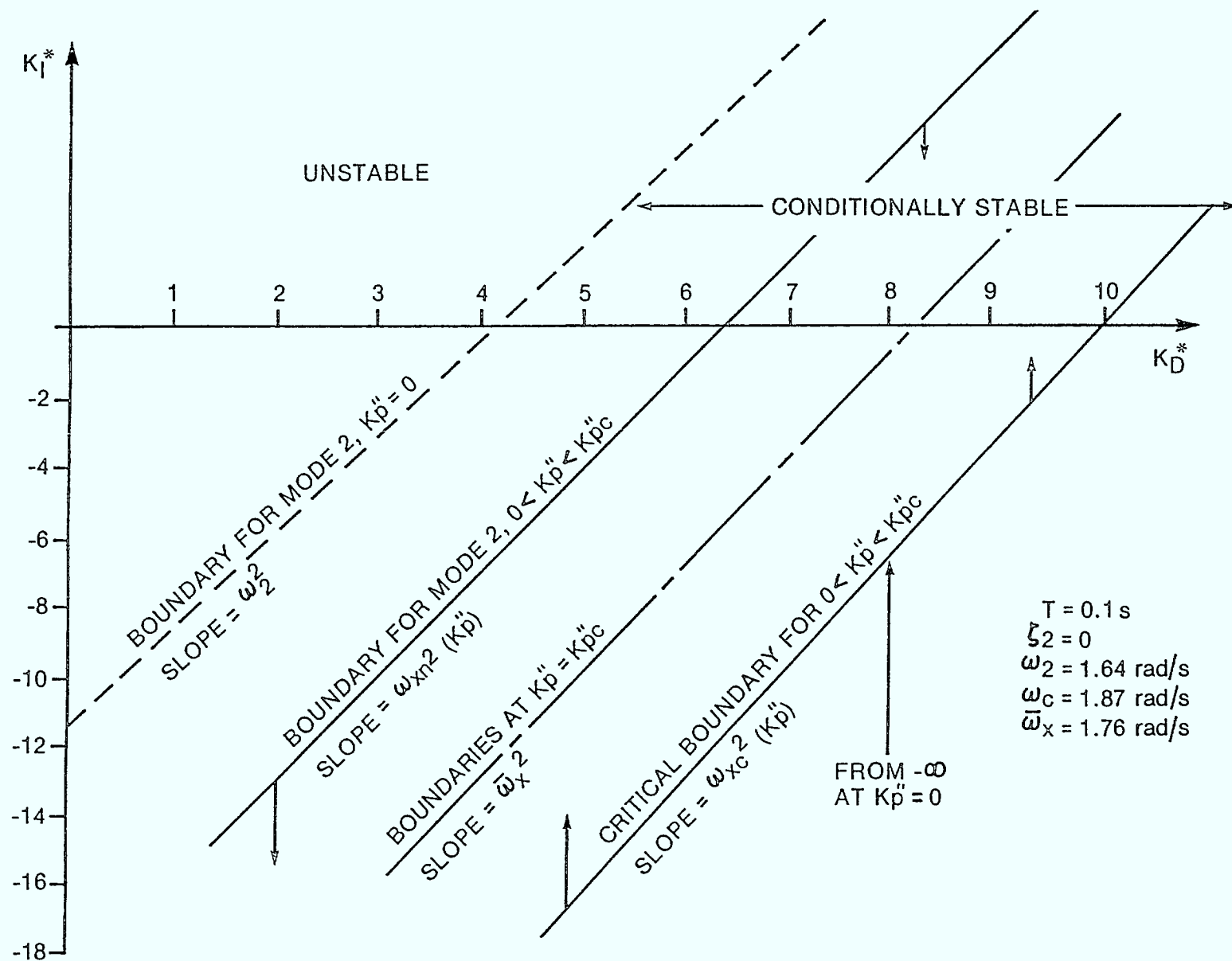
Figure 19   Stability Diagram With $\omega_2 < \omega_{c2}$ (T = 0.1 s)
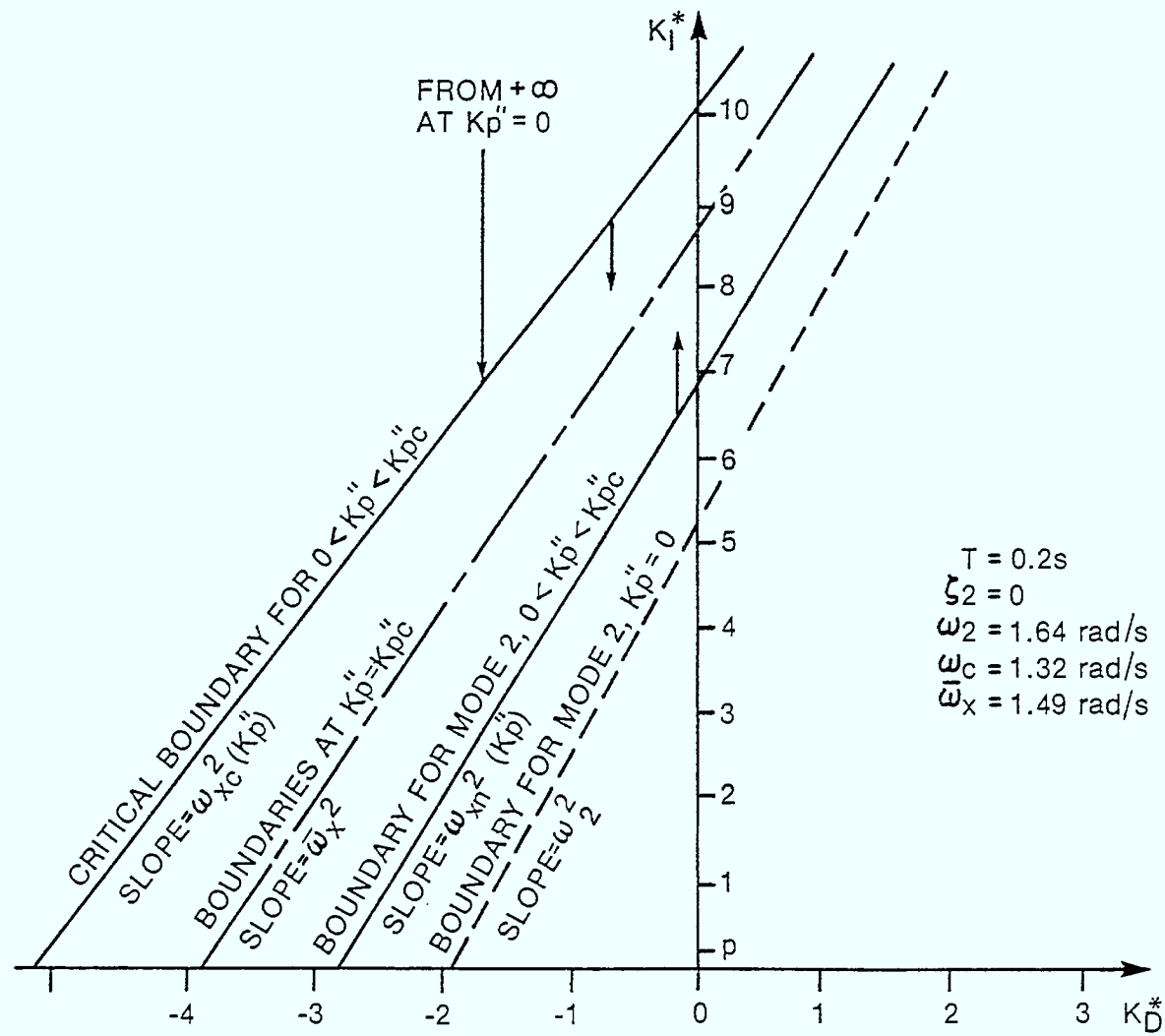
Figure 20   Stability Diagram with $\omega_2 > \omega_c$, (T = 0.2 s).

This time, the modal boundary moves up with a decreasing slope and the critical boundary approaches from $K_I^* = + \infty$ slope with increasing slope. The two meet at $\bar{\omega}_x^2$, $\bar{\delta}_x^*$, $K_{pc}"$. A design point providing rigid mode stability, ($K_D^* > 1$, $K_I^* <$ p are necessary conditions), can never be below the modal line and above the critical line at the same time. Consequently, mode n can never be stabilized when the rigid mode is stable. This concurs with the results in [2] where we had $K_I" < $ p and proved instability whenever $\omega_c < \omega_n < \pi/(2T)$.

In summary, a simple look at a graph of f_{SYS} ($\zeta_n = 0$) will show phase-unstable modes whenever their frequency ω_n is above the critical frequency ω_c (where $\Delta_T = 0$) and below $\pi/2T$. For modes with $\omega_n < \omega_c$, one must make sure that $K_p"$ is small enough ($< K_{pc}"$) for the $(-K_p")^{-1} \cos \omega T$ curve to cross f_{SYS}. Only then is a stable combination of K_D^* and K_I^* possible.

For the more general case ($\zeta_n \neq 0$), the results in Sections 3 and 4 provide an explanation to the changes in the stability boundaries. Damping was shown to have a stabilizing effect by moving the boundary towards the unstable region. When it is large enough, even a phase-unstable mode (Figure 20) can eventually have a (system) stable region, as proved in [2].

(b) Wheel Torque Limiters

The effect of torque saturation at the input of the reaction wheel has been treated in [6]. The conclusion was that large pointing errors ($> 1°$ in roll) take longer to be corrected and during that time, the controller integrator builds up a large signal that eventually destabilizes the spacecraft. The remedy to this undesirable behaviour was the introduction of a limiter in the integrator output. We now discuss this phenomenon in terms of stability regions.

Since the instability was associated with the rigid mode, we will study its diagram, shown on Figure 12. As pointed out earlier, the control designer must choose K_I^* and K_D^* in Region 1 for unconditional stability (i.e. for all gains $K_p"$). Note that this region is limited by $K_D^* = 1$ and $K_I^* = p = \omega_m \omega_f$. The effect of a torque limiter on the diagram is investigated by first considering the transfer function between the wheel torque input T_c and output T_M (Figure 1).

Let k_L represent the equivalent gain of the nonlinear saturation element. It can be shown that:

$$\frac{T_M}{T_c} = \frac{s\,k_L}{s + \omega_{mL}} \tag{70}$$

where we now have:

$$\omega_{mL} \overset{\Delta}{=} g k_L + 1/\tau_w, \tag{71}$$

and, consequently, from Eqs. (8):

$$p_L = \omega_{mL}\,\omega_f \ ,$$

$$\sigma_L = \omega_{mL} + \omega_f \ . \tag{72}$$

As the pointing error increases, large torques are demanded and k_L goes from unity to zero. At the limit, we have:

$$\lim_{k_L \to 0} p_L = \omega_f/\tau_w \ . \tag{73}$$

From Eq. (71), it is clear that the wheel speed measurement feedback gain g gradually looses its stabilizing effect as k_L goes to zero. From Eqs. (72) – (73), the upper limit of the stable Region 1 moves from $p=(g+1/\tau_w)\,\omega_f$ to $p_L=\omega_f/\tau_w$. For LSAT Roll ($\omega_f \approx 0.25$ rad/s), this represents a decrease by a factor of 23: from $0.0261s^{-2}$ to $0.0011s^{-2}$. $K_I{}^* = 0.0074s^{-2}$ from Appendix 1. In Figure 12, Region 1 shrinks to an unacceptable level: the design point ($K_I{}^*$, $K_D{}^*$) is now in Region 2. Furthermore, the overall controller gain, given by $K_p{}''k_L$, from Eq. (70), goes to zero as well. Region 2s of Figure 12 vanishes as the boundary (slope $\sim K_p{}''k_L$) becomes a horizontal line. The design point is now in Region 2u: the system is unstable.

The obvious solution to the problem is to lower the design point in Region 1, i.e., decrease $K_I{}^*$ to a value below ω_f/τ_w. As this value for $K_I{}^*$ is unacceptable under normal pointing errors conditions (see [6]), the decrease in $K_I{}^*$ should only occur when the boundary becomes close to the design point. This occurs at a value k_{Lx} defined in [6]: a subsequent decrease in k_L (i.e. increase in pointing error) would bring instability. Therefore, an integrator output limiter must start to decrease $K_I{}^*$ at this very point and ensure that its rate of decrease is greater than that of the boundary at p_L. This was accomplished in [6]. The effects of a torque limiter and integral loop limiter can thus clearly be visualized in terms of a stability diagram.

This section has shown that the method presented in this study allows the analysis of systems with loop delay and non-linear elements.

6. Conclusions

A general method for design and analysis of PID controllers for flexible spacecraft has been presented. It can handle as many modes as desired, in constrained or unconstrained form; an exact transformation between the two sets is carried out by the software. The usual assumption of mode separability and the approximate relations between constrained and unconstrained model parameters are consequently avoided. The definition of a 'system function' has the following advantages:

- it is dependent on the spacecraft properties and invariant under controller parameter changes,

- it allows the determination of the system stability boundaries and gives insight into its behaviour even before consideration of the controller gains,

- given constrained modal parameters, it provides accurate unconstrained modal frequencies via graphing vs frequency,

- it allows the definition of a 'mode separability assumption criterion',

- it illustrates the stabilizing effects of structural damping and flexibility filters and allows their analysis,

- it can be used in the investigation of systems with loop delay and nonlinear elements.

The numerical determination of two variables, ω_x, and δ_x^*, is sufficient to define the stability regions of the system. Analytic, closed-form results are also presented in order to clarify how these boundaries vary with controller gain.

A criterion was derived for the assessment of the assumption of mode separability. It was shown that the presence of other modes can have a stabilizing effect on a given mode.

The method presented in this study was applied to the analysis of LSAT. Because it uses an 'exact' (limited by computer capabilities) transformation from constrained to unconstrained modes, its results should improve on those presented by BAe[5].

Although current designs are aimed at filtering the flexible modes out of the controller bandwidth, it would be interesting to extend this method to third generation spacecraft and other types of controllers.

References

1. Hughes, P.C., Abdel-Rahman, T.M., "Stability of Proportional-Plus-Derivative-Plus-Integral Control of Flexible Spacecraft", J. Guidance and Control, Vol. 2, 1979, p. 499.

2. de Lafontaine, J., "Stability Analysis of the LSAT Normal Mode Controller", CRC Memo 1970-1 (DSM), 9 August 1983.

3. Millar, R.A., Vigneron, F.R., "The Effect of Structural Flexibility on the Stability of Pitch for the Communications Technology Satellite", presented at the Canadian Conference on Automatic Control, University of British Columbia, 23-24 June 1975.

4. Hughes, P.C., "Dynamics of Flexible Vehicles with Active Attitude Control", Celes. Mech. 9, 1974, 21-39.

5. BAe Dynamics Group, "Normal Mode Design and Analysis", LCS/PWN/0142/BAe, October 1982.

6. de Lafontaine, J., "Analysis of Nonlinear Effects in the LSAT Normal Mode Controller", CRC Memo 5310-1 (DSM), 7 September 1983.

APPENDIX 1

LSAT ROLL PARAMETERS

$I \quad = \quad 9875 \ \text{kg-m}^2$

$K_D^* = 2.807$

$\tau_w\dot{} \quad = \quad 220 \ \text{s}$

$K_I^* = 7.386 \times 10^{-3} \ \text{s}^{-2}$

$g \quad = \quad 0.1 \ \text{s}^{-1}$

$p \quad = 26.136 \times 10^{-3} \ \text{s}^{-2}$

$\omega_f \quad = \quad 0.25 \ \text{rad/s}$

$K_p'' = \quad 3.770 \times 10^{-3} \ \text{s}^{-2}$

n	$\Omega_n(\text{rad/s})$	K_n	$Z_n = 0.003$
1	0.999	0.000950	
2	1.081	0.613892	
3	1.093	0.012468	
4	1.998	0.051389	
5	2.256	0.000001	
6	2.746	0.000004	
7	3.085	0.008616	
8	3.707	~ 0.0	
9	4.229	0.000060	
10	4.725	~ 0.0	
11	5.102	0.000453	
12	5.360	~ 0.0	

LKC
TK5102.5 .C673e #1372
c.2
Stability analysis of
flexible spacecraft with PID
controller